A STUDY OF "SHEAR LAG" PHENOMENON IN A STIFFENED FLAT PANEL BY PHOTOELASTIC METHODS.

by

Hsu Tsi Fan

In Partial Fulfillment of the Requirements for the Degree of Master of Science in Aeronautical Engineering

California Institute of Technology

Pasadena, California

1939

ACKNOWLEDGEMENT

The author wishes to express his gratitude to Drs. Theodore von Karman and E.E. Sechler for the suggestion of this research subject and their helpful criticism during the course of the work. Grateful acknowledgement is also made to Dr. H.S. Tsien for his constant help during the year.

REFERENCES

(1) W.N. Bell and J.K. Bussey:

A Photoelastic Investigation of the Distribution of Shearing Stresses in a Stiffened Flat Panel

M.S. Thesis at California Institute of Technology, 1938

(2) C. Maxwell: Trans. Roy Soc., Edinburgh, Vol. 20, 1850

See also Timoshenko, Theory of Elasticity, p. 128

(3) Timoshenko: Theory of Elasticity, p. 129

(4) R.D. Mindlin: A Review of the Photoelastic Method of Stress Analysis, I. Journal of Appl. Phy. Vol. 10, pp. 222-241, 1939

(5) M.M. Frocht: Recent Advances in Photoelasticity

Trans. A.S.M.E., Vol. 53, pp. 135-153, 1931

(6) G.H. Lee and C.W. Armstrong: Effect of Temperature on Physical and Optical Properties of Photoelastic Materials.

Trans. A.S.M.E. Vol. 60, pp. A11-A12, 1938

(7) A.G. Solakian: Discussion on E.E. Weibel's Studies in Photoelastic Stress Determination, Vol. 56, pp. 652-653, 1934

INTRODUCTION

In the construction of modern metal airplanes there are many locations where a more or less concentrated load is transferred to a large area of material. Therefore the design-engineer is frequently confronted with the problem of "shear lag". This problem can be treated in a few simple cases by the mathematical theory of elasticity, especially by Airy's stress functions, but in many other cases, in order to avoid mathematical complexities, certain assumptions must be made which will simplify the analytical solution of the problem. These assumptions usually do not agree with the actual conditions therefore the results are not adequate. By the photoelastic method, however, the results obtained by the mathematical theory can be checked. It is the purpose of this experiment to check the results which have been obtained by the theoretical investigation for a few simple cases.

1) Propagation of light in isotropic and crystalline media.

Optical wave theories describe light as a transverse wave motion. The wave front of an optical disturbance advancing through a transparent medium is considered to be plane in the neighborhood of any point in the medium. In an isotropic medium there is only one wave velocity and it is the same regardless of the direction of travel of the light. In a crystalline medium, however, there are two wave velocities for each wave normal and these two velocities are different for wave normals through the point, in different directions. This is the phenomenon of double refraction. Therefore there will be two parallel wave fronts for each wave normal, furthermore, each of the waves is plane-polarized; that is, the vibration corresponding to each of the waves lies in a plane, and the two waves are perpendicular to each other and to the wave normal. If light of wave-length λ is passed at normal incidence through a crystalline plate of thickness d, the two resulting plane-polarized waves undergo phase retardations, Δ_1 and Δ_2, with respect to an unimpeded wave, given by

$$\Delta_1 = \frac{2\pi d}{\lambda}(n_1 - n)$$
$$\Delta_2 = \frac{2\pi d}{\lambda}(n_2 - n) \qquad (1)$$

where n is the index of refraction of the medium outside the plate and Δ_1 and Δ_2 are measured in radians. Their relative phase difference Δ is:

$$\Delta = \Delta_1 - \Delta_2 = \frac{2\pi d}{\lambda}(n_1 - n_2) \qquad (2)$$

2) The photoelastic effect.

It was discovered by Brewster, that almost all transparent materials, when stressed, become optically doubly refracting, and later Maxwell observed that the relation between stress and double refraction is similar to the stress and strain relation. Therefore, we may write, by analogy with the stress and strain relation:

$$\begin{aligned} n_1 - n_0 &= C_1 P + C_2 Q \\ n_2 - n_0 &= C_1 Q + C_2 P \end{aligned} \qquad (3)$$

in which C_1 and C_2 are the stress-optical coefficients, P and Q are principal stresses respectively. n_0 is the original optical index of the unstressed material. Hence, if we measure the absolute phase retardations Δ_1 and Δ_2 we can calculate the principal stresses P and Q, and if we measure the relative phase retardation Δ we can calculate the principal stress difference P-Q, for from the eqs. 2 and 3 we have

$$\Delta = \frac{2\pi d C}{\lambda}(P-Q)$$

in which $C = C_1 - C_2$ is the relative stress optical coefficient. If we determine the directions of the principal axis of the optical symmetry, we shall have the directions of the principal stresses.

3) Test procedure:

a) Apparatus.

The apparatus consists of a light source, a polarizer, and an analyzer, with their respective quarter-wave plates, a camera, and a loading frame. Two spherical mirrors and condensing lenses are employed to give a large beam of light through the model. The two polaroids are mounted in individual stands free to rotate 180 degrees as required in determining the isoclinic lines. Attached to each polaroid is the quarter-wave plate inclined at 45 degrees to the axis of the polaroid. These quarter-wave plates are quickly detachable as the procedure demands. The camera is made of a wooden box attached with ordinary camera shutter and plate holder made to slide on a rail for focusing.

b) Model

The material used for making the model is Bakelite BT61893 manufactured by the Bakelite Corporation, 247 Park Avenue, New York City. Among the desirable properties of this material are: 1. linear stress-strain relation, 2. high modulus of elasticity, 3. physical and optical homogeneity, 4. high transparancy. The physical properties of this Bakelite is given by G.H. Lee and C.W. Armstrong (Ref. 6), Young s Modulus = 615 pounds per square in. Poissons Ratio $\simeq$ 0.373. Concerning the thickness of the model, it is understood that a true state of plane stress is only approximately simulated in a plate; however, the smaller the thickness of the plate in comparison with a representative linear dimension in the plane of the plate, the closer is the similarity. It is also true that the larger the thickness of the plate, in comparison with a representative linear dimension in the plane of the plate, the closer does the stress distribution approach a state of plane strain. It is only when the thickness and other dimensions of the plate are of the same order of magnitude that a two-dimensional state of the stress is not, in general, realized. In the present case the dimension of the plate is 3 × 5 in., the thickness of the plate is .23 in. The model is machined to the desired shape and the finishing is accomplished by coating the model with lacquer, thus saving the time of grinding and polishing.

c) Loading.

Creeping action in bakelite under moderately high stresses is one of the important phases of the physical properties of the material. A thorough study of the various characteristics of bakelite has been carried out at the Testing Laboratories of Columbia University, and it was pointed out by A.G. Solakian (Ref.7) that in a specimen $\frac{1}{4}$ inch in thickness, stresses corresponding to a fringe of eleventh order can be used safely. In the present case, the model is loaded in two different ways: Type I: The load is applied to the stiffener at the top and absorbed as a distributed load across the bottom.

Type II: The load is applied to the stiffener at the top and absorbed as a distributed load across the webs only.

The load applied in each type of loading is 2000 lbs. corresponding approximately to a maximum fringe order of eleven.

The loading frame in which the model is loaded consists of a machined flat as a base, a method of applying the load, and a means of determining the load. The loading beam is calibrated, giving dial reading against load. Some difficulty was found with the loading frame, therefore, if further experiments are to be made, a loading machine should be designed.

d) Network of Reference.

In order to transfer the observed isochromatic and isoclinic lines to the drawing board the photographic method is used.

1) Isochromatic lines.

Isochromatic lines by definition are the shear contour lines; i.e. lines along which the maximum shearing stress is a constant. The photographs of the isochromatic lines are taken by using the circularly polarized light. The light source is a monochromatic 60-watt Sodium Lab-Arc. The monochromatic light together with the quarter wave plates produce circularly polarized light and allows the isochromatic lines of the model to be observed without the presence of the isoclinic lines.

2) Isoclinic lines

The isoclinic lines lines by definition are the lines along which the directions of the principal stresses are constant. Previously (Ref. 1), these lines have been recorded by means of monochromatic light. Then the isoclinic lines can only be detected by comparing two plates, one taken with plane-polarized light and another taken with circularly polarized light. In order to eliminate this rather tedious work, the present author used plane-polarized white light and panchromatic photographic plates. In this case, the isochromatic lines will appear as bands of different color but of approximately the same intensity, therefore they will not be registered on the photographic plate when developed. Thus the record is not only easier to use but also more accurate. However in using white light, because of its strong intensity the model will be heated. The test performed by G.H. Lee and C.W. Armstrong (Ref. 6) on Bakelite BT61893 indicates that the relationship between the fringe order and the stress are linear over the temperature range from 20° to 140°F., however the effect of creep of the material is noticed at the temperature 96°-106°F. In order to avoid this undesirable effect a water cell made of glass is placed between the light source and the specimen. Complete series of isoclinic pictures are taken from zero to 90 degrees in 10 degree intervals by rotation of the polaroids and additional pictures were made in the range from 70° to 80° where the line changes rapidly.

3) Isotropic Points.

At an isotropic point, (Ref. 4) the parameter of the isoclinic is indeterminate. Hence all isoclinics pass through an isotropic point and there is some difficulty in constructing the isostatics in the neighborhood of such a point. Filon, Föppl and Neuber, and Von Mises have shown that the configuration of the isotropic point depends upon the number and orientation of the directions through the point for which a tangent to the isoclinic makes an angle with the x axis equal to the parameter of the isoclinic. There are one, two or three such asymptotic directions in the cases which occur most often. These types, with their corresponding isostatics, are illustrated in Figs. below :

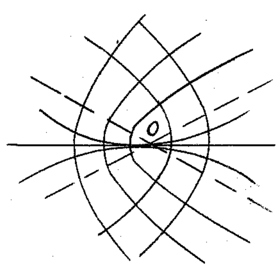
(1)

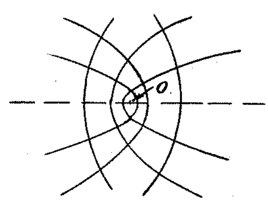
(2)

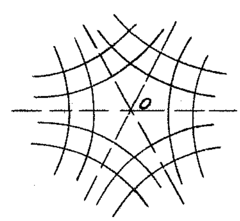
(3)

To determine to which type a particular isotropic point belongs, it is necessary to find the asymptotic directions. In the present cases there is one isotropic point on the right hand corner between the free edges, in each type of loading. In Fig. 4 The isoclinics through such a point are drawn to an enlarged scale. Calling ζ the angle which the isoclinic through O makes with the y axis and plotting a graph for which the parameter ϕ of the isoclinic is the abscissa and ζ is the ordinate. A line AB on this diagram meets the CD curve at a number of points equal to the number of asymptotic directions, in this case only one, at 81° Hence the isotropic point is of type 2.

4) Procedure of Calculation.

a) Principal stress trajectories.

The directional distribution of each of the principal stresses P and Q may be plotted after the isoclinic lines have been determined; the two systems forming a network of orthogonal curves.

b) Maximum shearing stress trajectories.

Since the maximum shearing stress at any point acts at an angle ϕ to the directions of P and Q the directional distribution of τ_{max} may be similarly plotted.

c) Separation of the principal stresses.

1) Calibration beam.

The fringe order of the photoelastic material is determined by applying a pure moment to a comparison beam. By using the flexure formula, the stress at any distance from the neutral axis is calculated, and hence the stress determination per fringe line is known; i.e.:

$$\sigma = \frac{My}{I}$$

Since $\sigma = P$ and $\theta = 0$ the expression for maximum shearing stress becomes:

$$\tau_{max} = \frac{\sigma}{2}$$

Therefore, the increment of shearing stress per fringe is the shearing stress at a given point divided by the fringe order n at the same point, that is,

$$\Delta \tau_{max} = \frac{\tau_{max}}{n}$$

From the work done by previous investigators (Ref. 1) on the same problem the $\Delta \tau_{max}$ has been determined with the same material of the same thickness (t =0.23 in.):

$$\Delta \tau_{max} = 206.6 \ \text{lbs/in}^2\text{/line}$$

This has been later checked with the case of the second type of loading. The shearing force at the stiffener calculated by using the above value, equals 927 pounds which is a quite satisfactory result comparing with 1000 pounds as it should be.

2) Determination of P-Q at any point.

We have obtained the values of P-Q on the isocromatics which correspond to a tint of passage, but in the case of a strained model, we require P-Q at other points. This is determined by taking pictures of isochromatic lines of progressive loading. Since the load is increased in the ratio

and the material obeys Hookes law (strained within elastic limit), all the stresses are in the same ratio. This gives P-Q; and we note that the point in question lay originally on the isochromatic of fractional order n/k. In this way the isochromatics of fractional orders can be plotted thus determines

P-Q at any point of the plate.

3) Determination of the separate stresses.

Two methods were used in determining the separate stresses. For the first type of loading a graphical-integration method is used which has been suggested by L.N.G. Filon (Ref. 2). The equations used in this method are given in the following forms:

$$P = P_0 + \int (P-Q) \cot.\psi \, d\phi$$
$$Q = Q_0 + \int (Q-P) \cot\psi_1 \, d\phi \qquad (4)$$

where ψ is the angle through which the stress trajectory of P at a point has to be rotated in order to bring it upon the isoclinic at the same point.

The values of P-Q and ψ for the various points having been found by method described, P-Q cot ψ can be calculated and plotted with respect to ϕ. The area of this diagram between any two angles ϕ can be found, thus gives $\int (P-Q) \cot.\psi \, d\phi$ which is equal to $P-P_0$. In this case the author has started from points on the free edge and followed inwards the line of P-principal stress since P is zero on the free edge. When P-stress is known everywhere on the plate the Q stress is calculated, since we know the value of P-Q everywhere on the plate. It is advisable to integrate along both principal stress lines to reach the same point, as a check on the accuracy of the work, however due to the limited time the author has only integrated along P-stress lines, and only a few points have been checked by integration along the Q-stress lines, the results agreeing satisfactorily with each other.

Another way of obtaining the principal stresses is by a calculation which was indicated first by Clark Maxwell (Ref. 3) From the equations of equilibrium for the case when no body forces are acting on the plate, we have:

$$\frac{\partial \sigma_x}{\partial x} = -\frac{\partial \tau_{xy}}{\partial y} \quad , \quad \frac{\partial \sigma_y}{\partial y} = -\frac{\partial \tau_{xy}}{\partial x}$$

from which we obtain by integration,

$$\begin{aligned} \sigma_x &= (\sigma_x)_0 - \int_0^x \frac{\partial \tau_{xy}}{\partial y}\, dx \\ \sigma_y &= (\sigma_y)_0 - \int_0^y \frac{\partial \tau_{xy}}{\partial x}\, dy \end{aligned} \tag{5}$$

In this case, the σ_x is equal to zero at the free boundaries, therefore, our equation can be written as

$$\sigma_x = \int_x^h \frac{\partial \tau_{xy}}{\partial y}\, dx \tag{6}$$

where h is width of the plate. In order to find the shearing stress, consider the condition of equilibrium of a small triangular prism fig. 1 and 2.

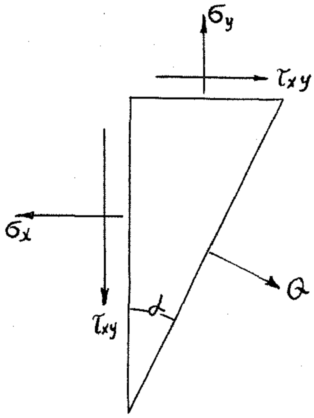

FIG. (a)

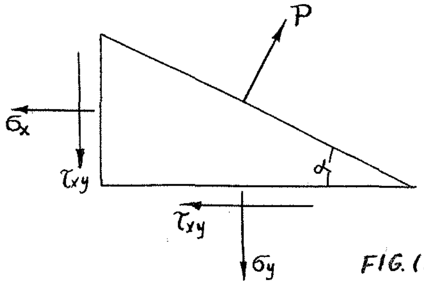

FIG. (b)

From Fig. (a) we have:

$$-\sigma_x + \tau_{xy} \tan\alpha + Q \cos\alpha \frac{1}{\cos\alpha} = 0$$

$$-\tau_{xy} + \sigma_y \tan\alpha - Q \sin\alpha \frac{1}{\cos\alpha} = 0$$

Hence we have:

$$-\sigma_x + \tau_{xy} \tan\alpha + Q = 0 \qquad (7)$$

$$\sigma_y - \tau_{xy} \operatorname{ctn}\alpha - Q = 0 \qquad (8)$$

From Fig. (b) we have:

$$-\sigma_x \tan\alpha - \tau_{xy} + P \sin\alpha \frac{1}{\cos\alpha} = 0$$

Hence we have:

$$-\sigma_x - \tau_{xy} \operatorname{ctn}\alpha + P = 0 \qquad (9)$$

From equations 7 and 9 we have:

$$\tau_{xy} (\tan\alpha + \operatorname{ctn}\alpha) = P - Q$$

Therefore the shearing stress is equal to:

$$\tau_{xy} = \frac{P-Q}{2} \sin 2\alpha \qquad (10)$$

Integrating $\frac{\partial \tau_{xy}}{\partial y}$, $\frac{\partial \tau_{xy}}{\partial x}$, graphically along the X and Y axes, σ_x and σ_y at each point can be calculated by equation (5) and knowing the shearing stress τ_{xy} at those points by equation (10) we can find the principal stresses P and Q by using Mohr's circle or by the relations:

$$P = \frac{\sigma_x + \sigma_y}{2} + \sqrt{\left(\frac{\sigma_x - \sigma_y}{2}\right)^2 + \tau_{xy}^2}$$

$$Q = \frac{\sigma_x + \sigma_y}{2} + \sqrt{\left(\frac{\sigma_x - \sigma_y}{2}\right)^2 + \tau_{xy}^2}$$

The author has developed a method directly from this by which the P and Q can be obtained by a single integration. From equations(7) and (8) we get:

$$\sigma_x - \sigma_y = \tau_{xy} \left(\tan\alpha - \mathrm{ctn}\,\alpha\right) = -\tau_{xy}\, \mathrm{ctn}\,\alpha$$

therefore, substituting the value of τ_{xy} from equation (10):

$$\sigma_x - \sigma_y = -\frac{(P-Q)}{2} \cos 2\alpha \qquad (11)$$

From the equations (8) and (9) the following relation is obtained:

$$\sigma_x + \sigma_y = P + Q \qquad (12)$$

Therefore by integrating along X axis only σ_x is obtained, and knowing σ_x by the equation (11) σ_y can be found. Then using equation (12) the sum of the principal stresses

P - Q can be calculated. Since P-Q is known from the evaluation of the isocromatics, therefore the separate stresses can be easily calculated by simple addition and subtraction.

CONCLUSION

The model used in this project has been investigated sufficiently to give a complete picture of the stress characteristics of the sheet reinforced with a stiffener. In calculating the separate stresses the author finds the second method is more suitable, since the slope of the one curve, namely $\frac{\partial \tau_{xy}}{\partial y}$, is easier to find than the angle between the slopes of two curves, namely the slope of the principal stress lines and the isoclinics. Furthermore in the first case $\cot \psi$ is involved which is liable to give considerable error if the angle is inaccurately measured. But in the second case only $\sin \alpha$ and $\cos \alpha$ are involved which would not give too much error in case the angle measured is little off of its proper value.

APPENDIX A.

<u>Photographs.</u> Pertinent data is given on each picture. The following photo-elastic photographs are shown:

Pages	1 - 111.	The model under progressive stages of Type I loading (isochromatics).
Pages	1V - V111.	Isoclinics of the model under Type I loading.
Pages	1X - X1V .	Isochromatics and isoclinics of the model under Type II loading.

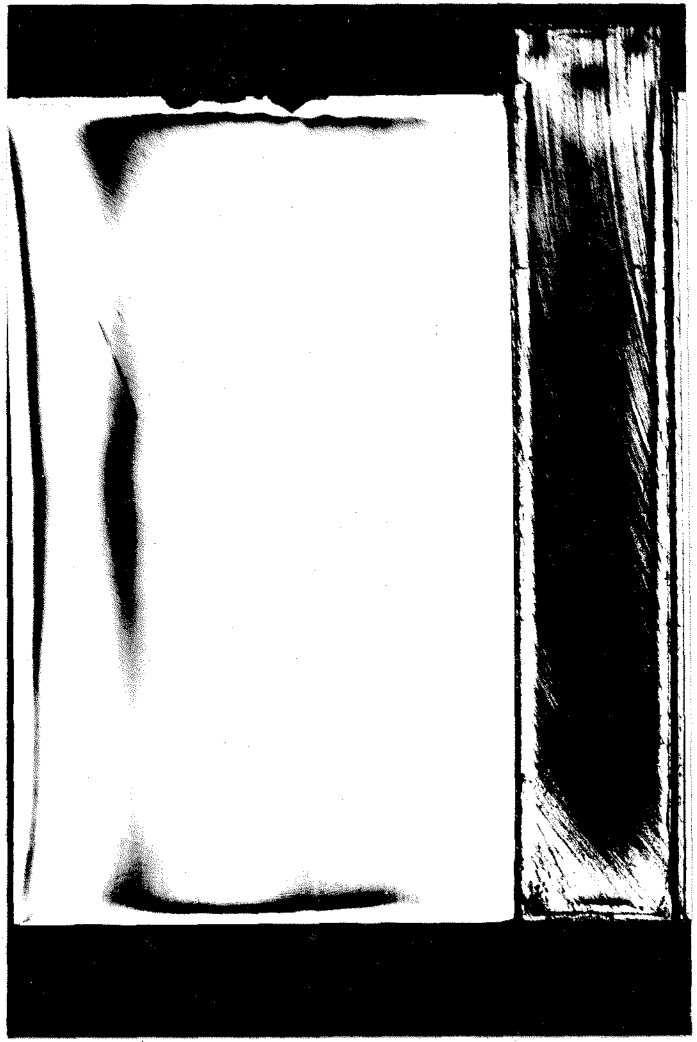

1 A P = 0

2 A P = 400 lbs

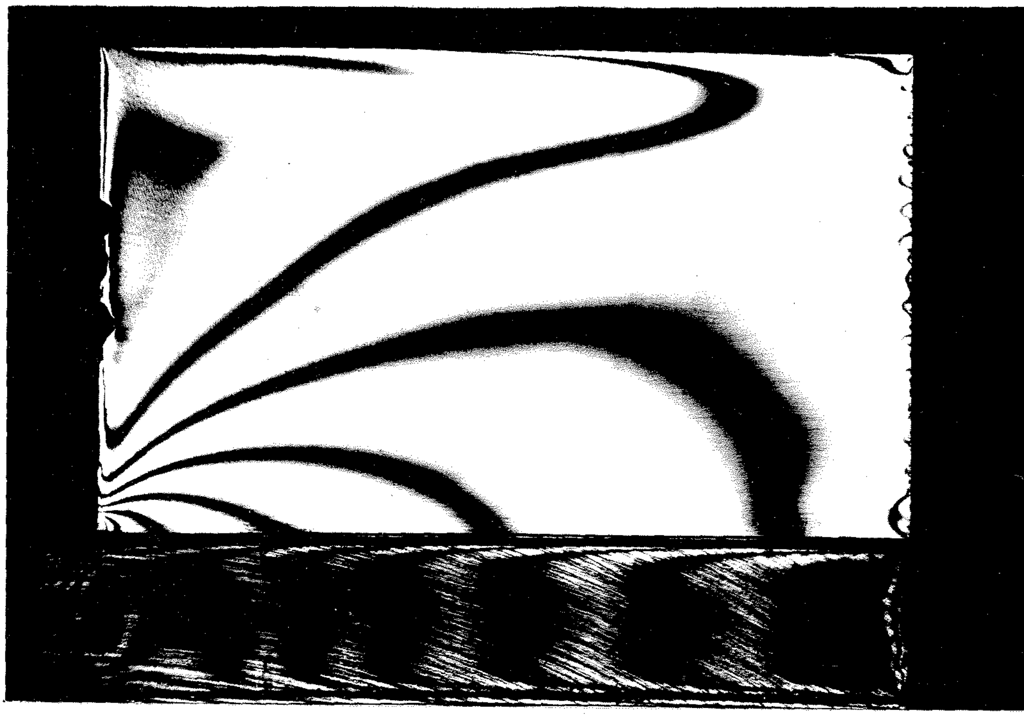

4A P = 1200 lbs

3A P = 800 lbs

Table III (continued)

(1) x/h_1	(2) y/h_2	(3) τ_{xy}	(4) $(\sigma_x-\sigma_y)$	(5) σ_x	(6) σ_y	(7) $(P+\theta)$	(8) $(P-\theta)$	(9) P	(10) θ
1.0	.5	0	465	0	-465	-465	475	5.0	-470
.9	.5	71.6	352	6.52	-345.5	-339	420	40.5	-379.5
.8	.5	160.0	447	27.00	-420.0	-393	550	78.5	-471.5
.7	.5	250.0	708	47.85	-660.2	-612.3	832	109.85	-722.2
.6	.5	336.6	900	62.85	-837.2	-774.3	1115	170.35	-944.7
.5	.5	417.3	1016	59.90	-956.1	-896.2	1318	210.9	-1107.1
.4	.5	488.0	1135	22.10	-1112.9	-1090.8	1502	205.6	-1296.4
.3	.5	533.3	1325	26.7	-1351.7	-1378.4	1685	153.3	-1531.7
.2	.5	552.7	1506	70.7	-1576.7	-1597.4	1838	120.3	-1717.7
.1	.5	560.0	1617	108.7	-1725.7	-1834.4	1945	55.3	-1889.7
.0	.5	560.8	1665	140.0	-1805	-1945	2018	3.65	-1948.7
1.0	.6	0.0	290	0	- 290	- 290	310	10	- 300
.9	.6	48.0	222	16.93	- 205.1	- 188.2	275	43.4	- 231.6
.8	.6	112.7	316	40.7	- 275.3	- 234.6	380	72.7	- 307.3
.7	.6	212.0	483	66.8	- 416.2	- 349.4	636	143.3	- 492.7
.6	.6	350.0	633	81.5	- 551.5	- 470.0	928	229.0	- 699.0
.5	.6	475.3	760	78.2	- 681.8	- 603.6	1192	294.2	- 897.8
.4	.6	565.3	905	58.7	- 846.3	- 787.6	1436	324.2	-1111.8
.3	.6	623.4	1145	27.4	-1117.6	-1090.2	1672	290.7	-1381.1
.2	.6	645.3	1400	42.7	-1442.7	-1485.4	1883	198.8	-1684.2
.1	.6	638.7	1627	112.6	-1739.6	-1852.0	2053	100.5	-1952.5
.0	.6	608.0	1815	169.9	-1984.9	-2154.8	2190	17.6	-2172.4
1.0	.7	0.0	86	0.0	- 86	- 86	170	42	- 128
.9	.7	6.66	50	22.8	- 27.2	- 4.4	67	31.3	- 35.7
.8	.7	60.0	190	59.9	- 130.1	- 70.2	187	58.4	- 128.6
.7	.7	180.6	300	86.6	- 213.4	-126.8	427	150.1	- 276.9
.6	.7	320.0	290	117.2	- 172.8	- 55.6	694	319.2	- 374.8
.5	.7	453.3	290	161.0	- 129.0	32	956	494.0	- 462.0
.4	.7	574.5	400	199.2	- 200.8	- 1.6	1248	623.2	- 624.8
.3	.7	733.3	694	200.0	- 494.0	-294	1618	662.0	- 956.0
.2	.7	810.0	1145	127.7	-1017.3	- 889.6	1970	540.2	-1429.8
.1	.7	800.0	1600	35.2	-1564.8	-1529.6	2260	365.2	-1894.8
.0	.7	718.0	2100	-68.3	-2168.3	-2236.6	2489	126.2	-2362.8
1.0	.8	0.0	-100	0.0	100	100	0	50	50
.9	.8	0.0	-70	0.0	70	70	0	35	35
.8	.8	12.7	0	9.12	9.1	18.22	78	48.11	- 29.9
.7	.8	119.0	109	29.95	- 79.1	- 49.15	243	96.9	- 146.1
.6	.8	222.6	143	110.5	- 32.5	78.0	430	254	- 176.0
.5	.8	341.4	136	177.1	41.1	218.2	676	447.1	- 228.9
.4	.8	500.0	90	397.0	307	704.0	995	849.5	- 145.5
.3	.8	770.0	157	706.0	549	1255.0	1420	1337.5	- 82.5
.2	.8	930.6	412	953.0	541	1494.0	1957	1725.5	- 231.5
.1	.8	986.6	1000	873.0	- 127	746	2460	1603.0	- 857.0
.0	.8	1004.7	2650	646.0	-2004	-1358	2926	784	-1009.5

Table III (continued)

(1) x/h_1	(2) y/h_2	(3) τ_{xy}	(4) $\sigma_x - \sigma_y$	(5) σ_x	(6) σ_y	(7) $(P+Q)$	(8) $(P-Q)$	(9) P	(10) Q
1.0	.9	0	- 410	0	410	410	0	205	205
.9	"	0	- 250	0	250	250	0	125	125
.8	"	0	- 20	0	90	90	0	45	45
.7	"	14.6	- 10	5.07	- 4.9	.17	41	20.6	-20.4
.6	"	77.5	48	96.3	48.3	144.6	150	147.3	- 2.7
.5	"	143.0	52	192.7	140.7	333.4	330	331.7	1.7
.4	"	205.0	-100	422.0	522.0	944.0	580	762.0	182.0
.3	"	310.0	-240	932.0	1172.0	2104.0	965	1534.5	569.5
.2	"	733.4	-17	1270.0	1287.0	2557	1630	2093.5	463.5
.1	"	1316.7	450	1200.0	750.0	1950	2450	2200	-250.0
0	"	1455.0	3760	1019.0	-2741	-1722	3570	924	-2646.0

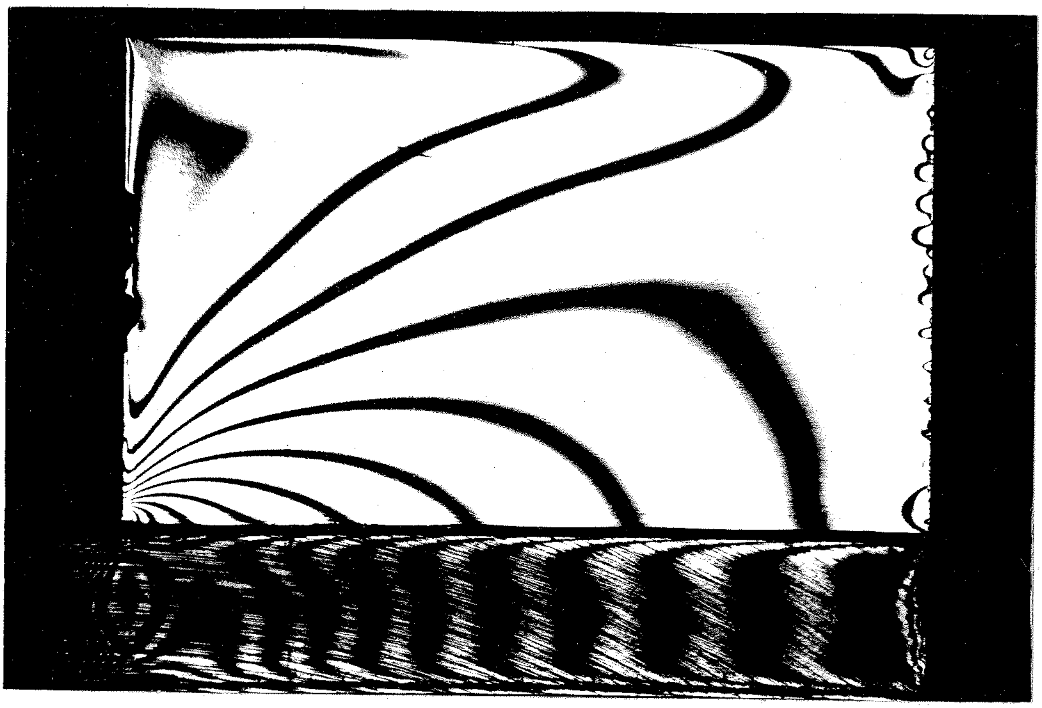

6 A P = 2000 lbs

5 A P = 1600 lbs.

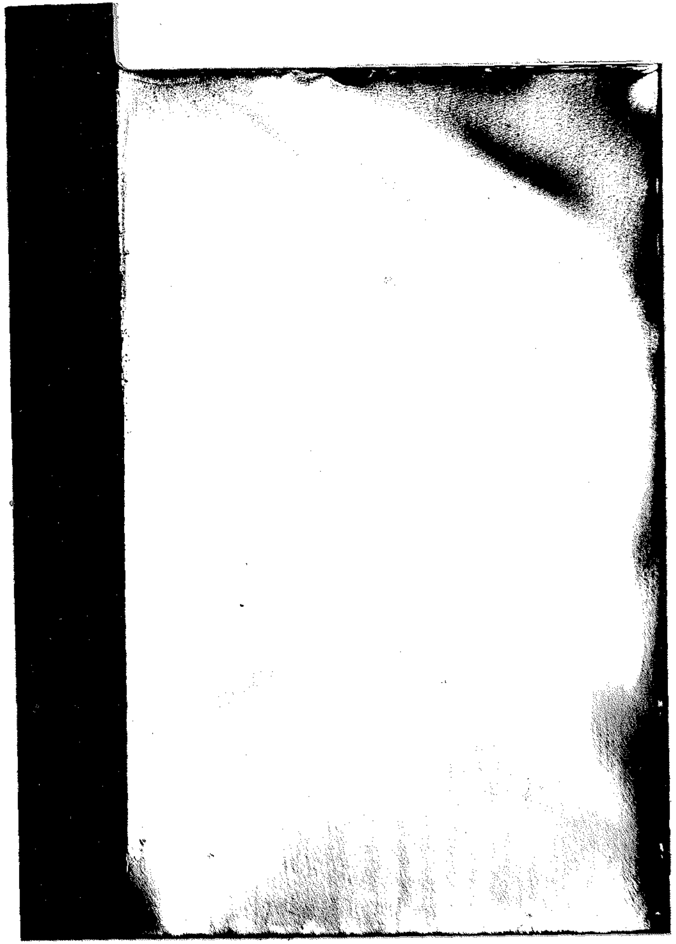

7A $P = 2000$ lbs $\alpha = 0°$

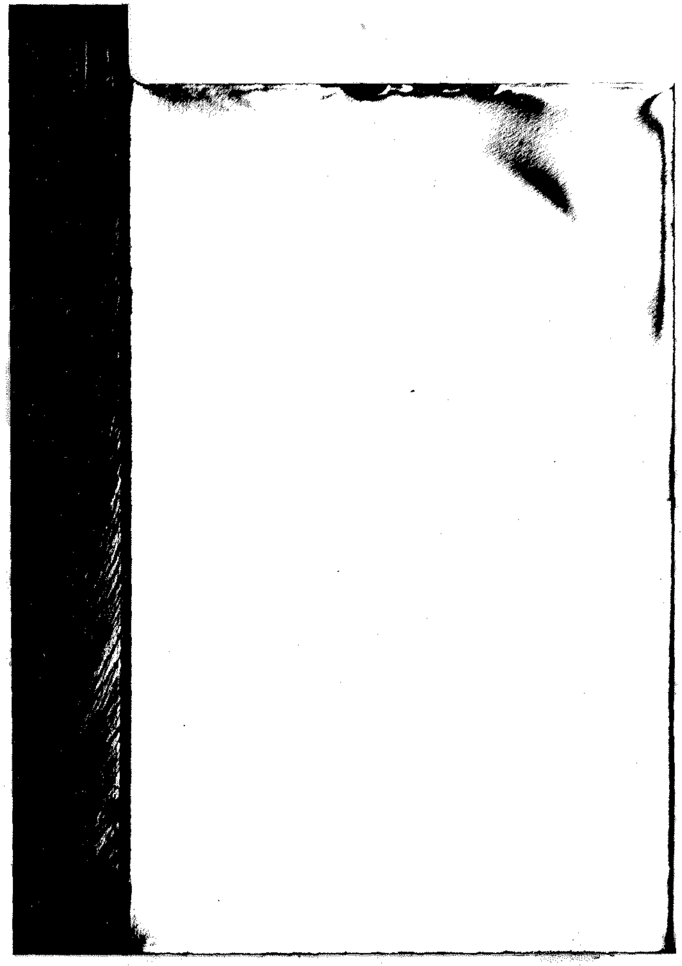

8A $P = 2000$ lbs $\alpha = 10°$

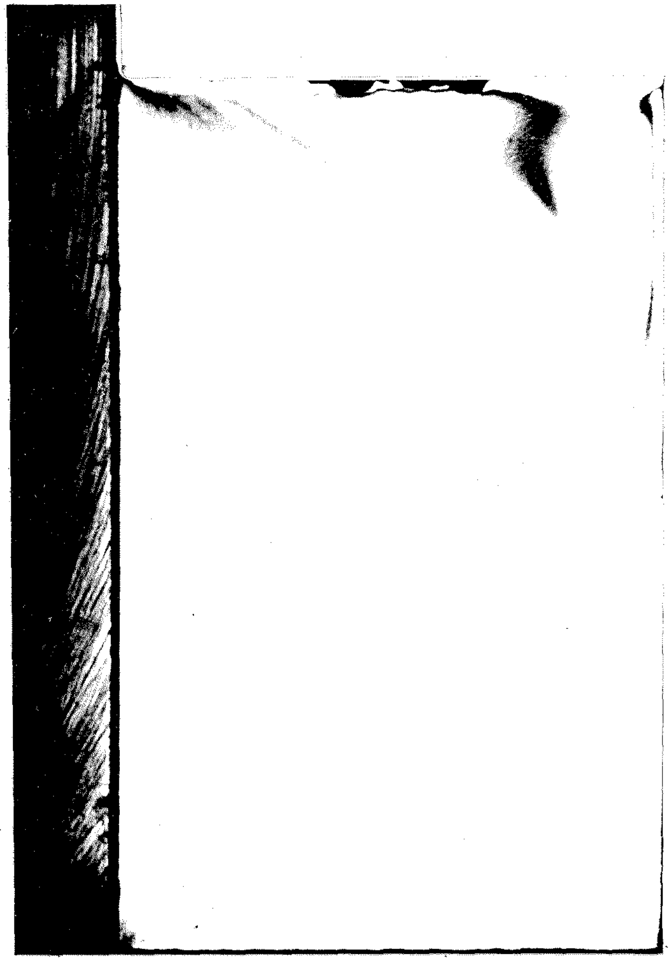

9A $P = 2000$ lbs $\alpha = 20°$

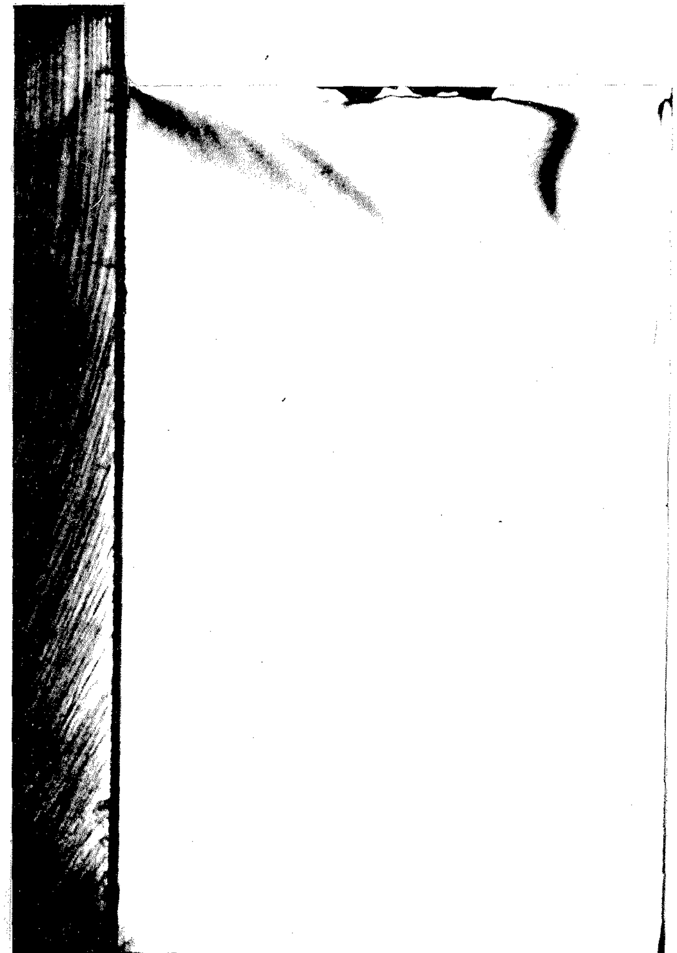

10A $P = 2000$ lbs. $\alpha = 30°$

V

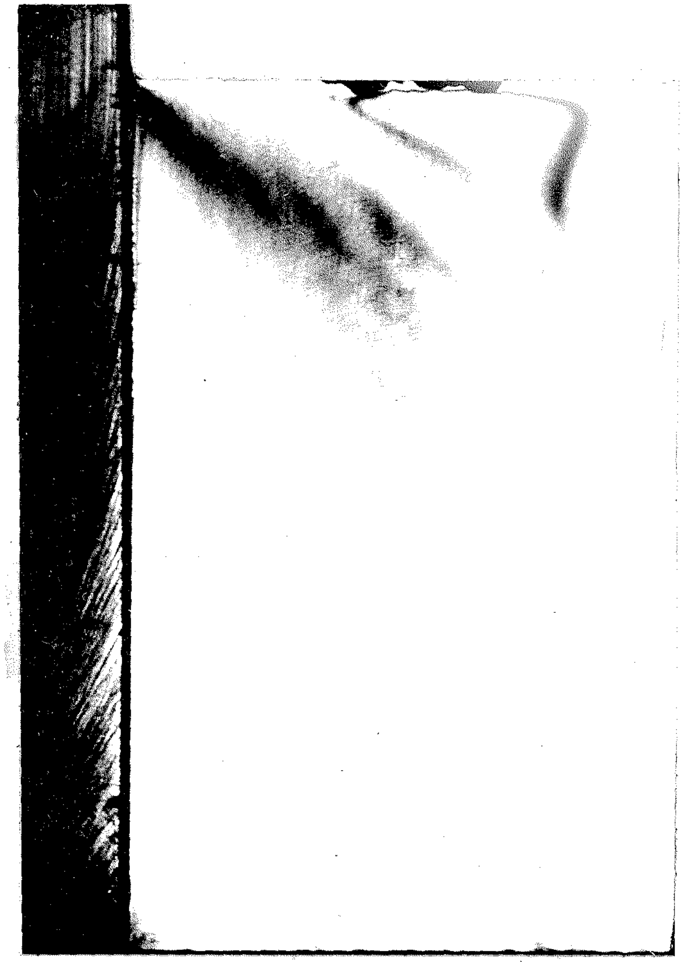

11 A $P = 2000$ lbs $\alpha = 40°$

12 A $P = 2000$ lbs $\alpha = 50°$

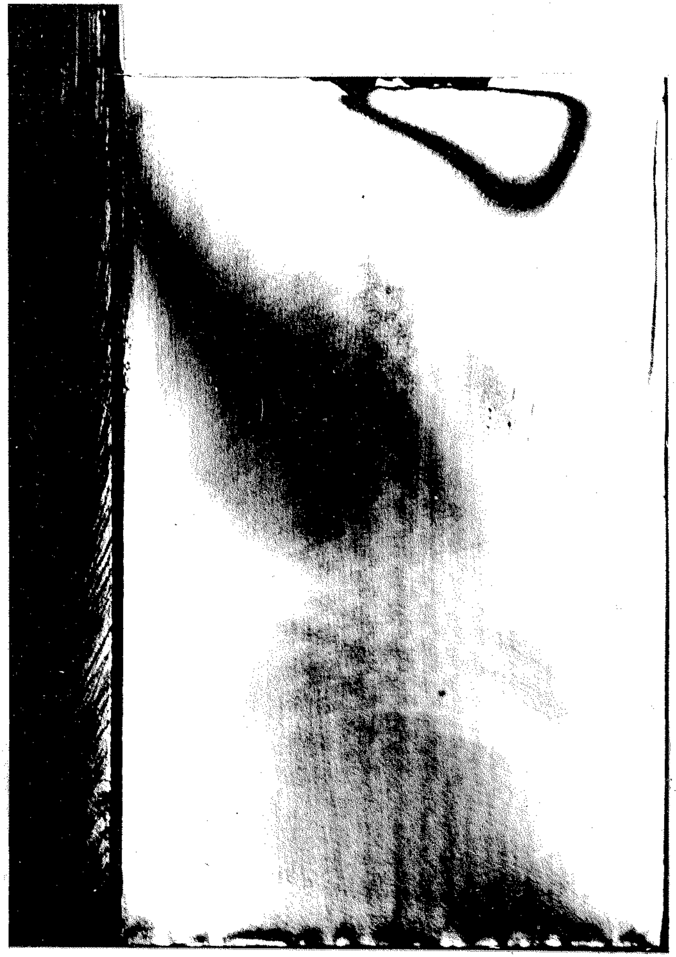

13A $P = 2000$ lbs $\alpha = 60°$

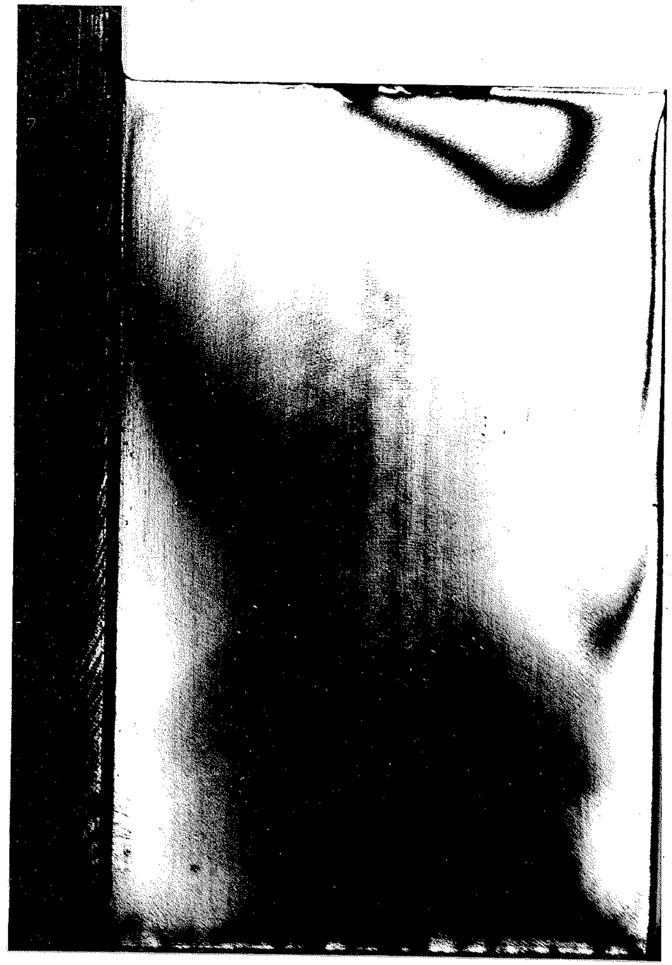

14A $P = 2000$ lbs $\alpha = 70°$

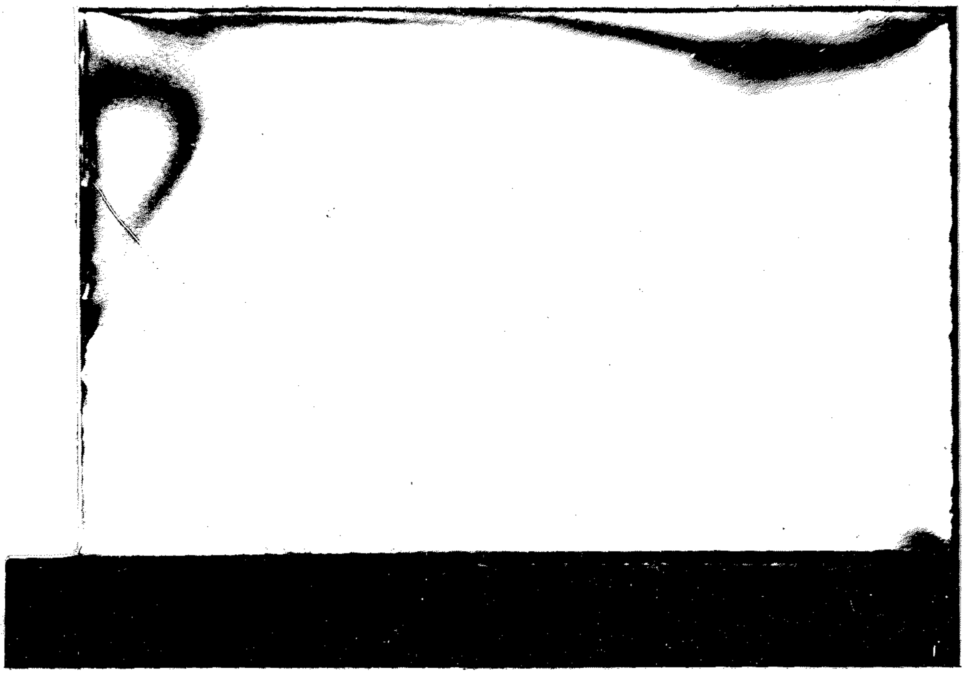

16 A P = 2000 lbs α = 80°

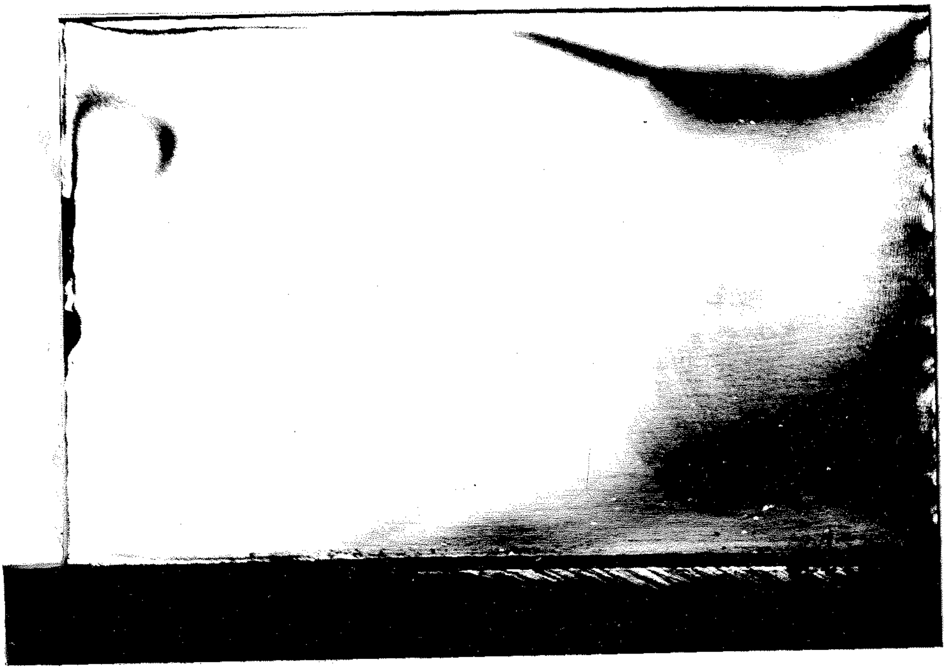

15 A P = 2000 lbs α = 75°

1 B P = 2000 lbs

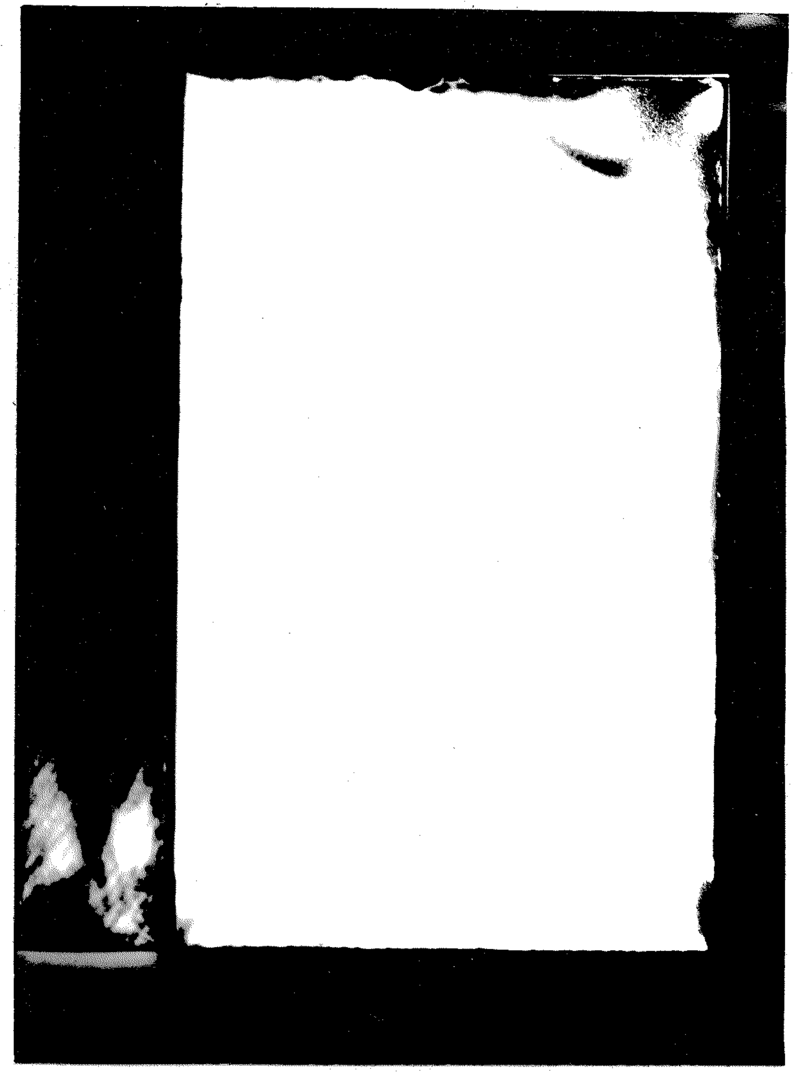

2 B P = 2000 lbs $\alpha = 0°$

X

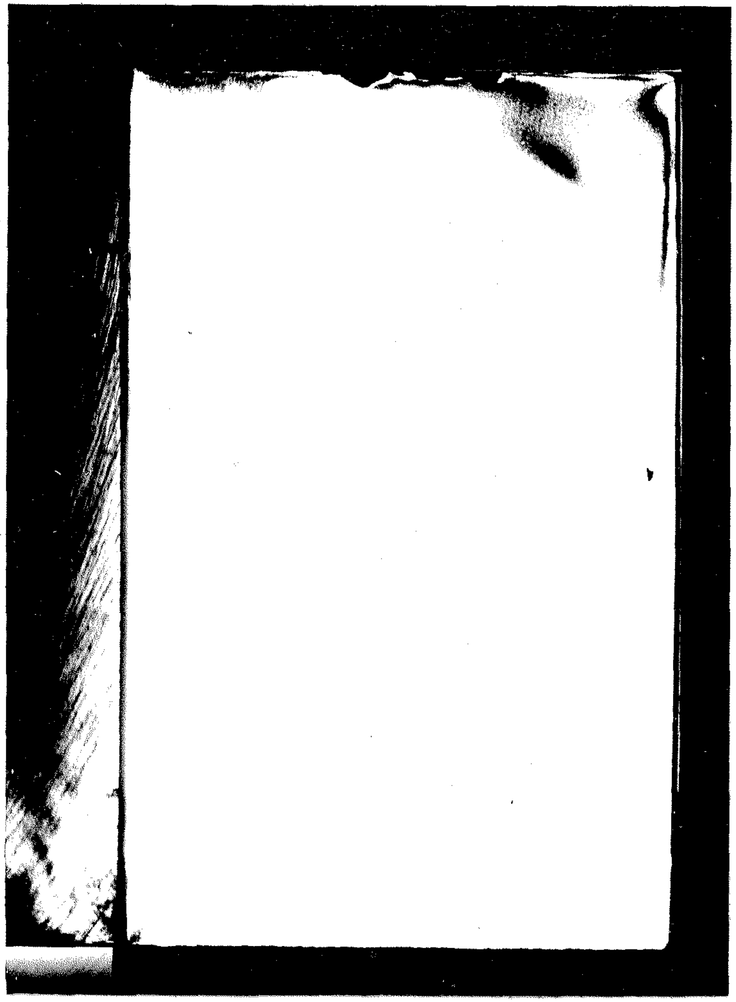

3B $P = 2000$ lbs $\alpha = 10°$

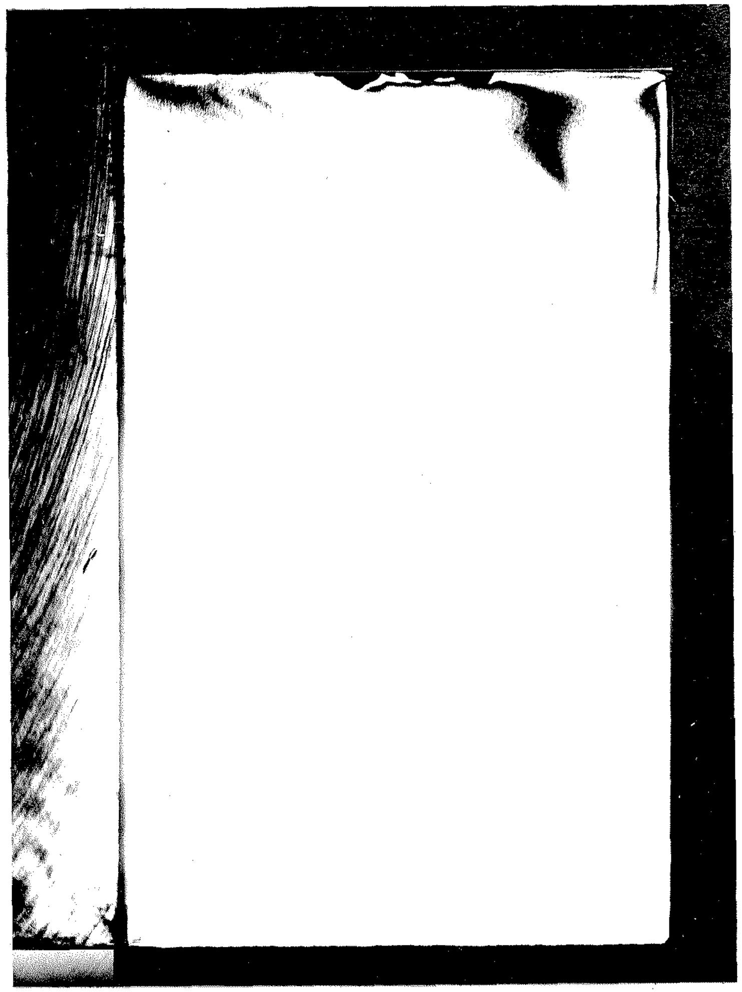

4B $P = 2000$ lbs $\alpha = 20°$

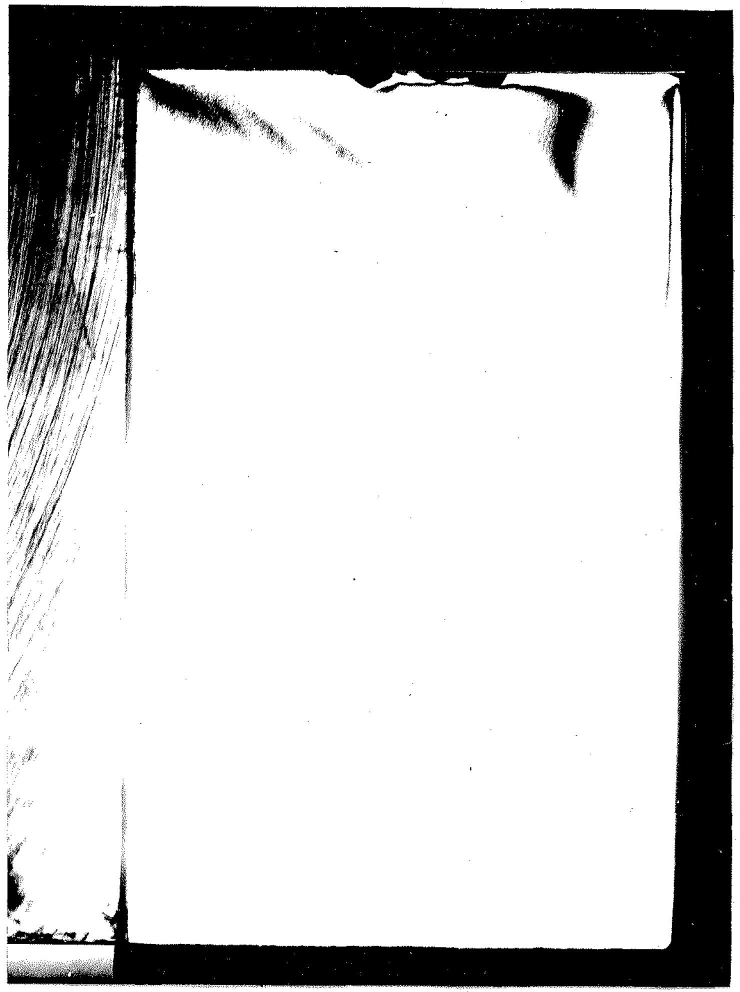

5B P= 2000 lbs $\alpha = 30°$

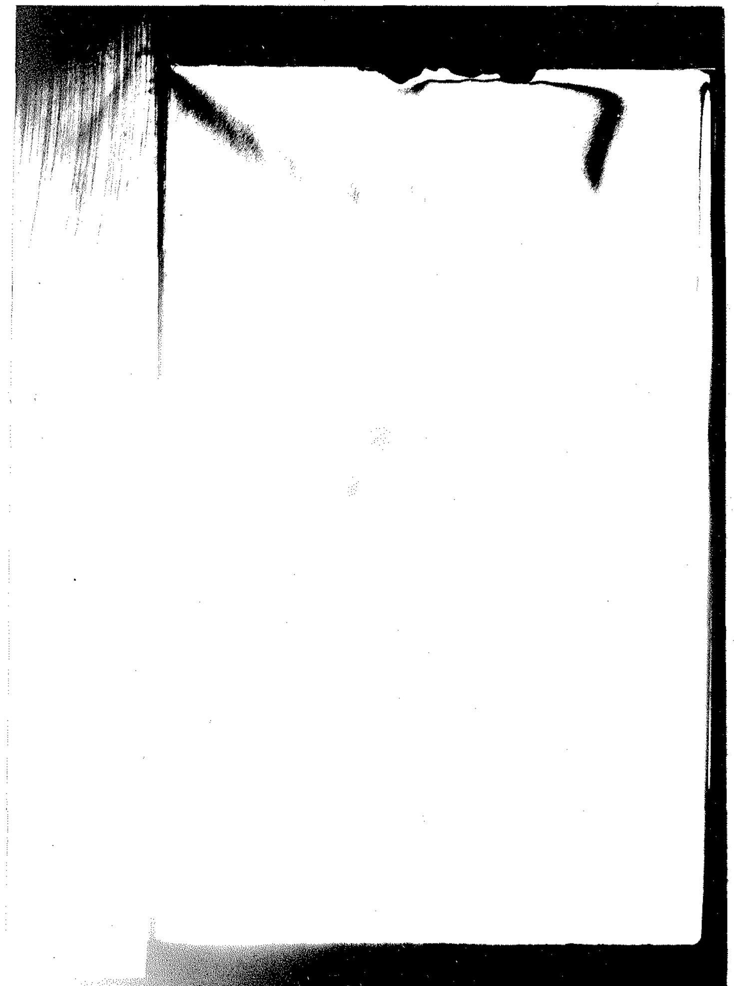

6B P = 2000 lbs $\alpha = 40°$

7B $P = 2000$ lbs $\alpha = 50°$

8B $P = 2000$ lbs $\alpha = 60°$

10B $P = 2000$ lbs $\alpha = 72.5°$

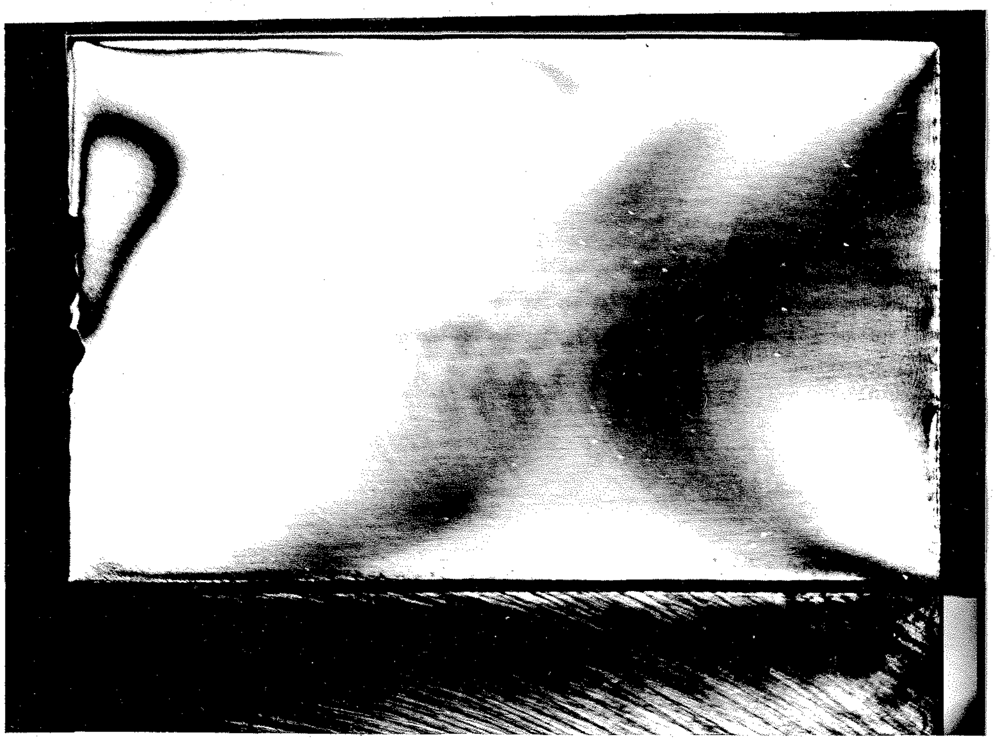

9B $P = 2000$ lbs $\alpha = 70°$

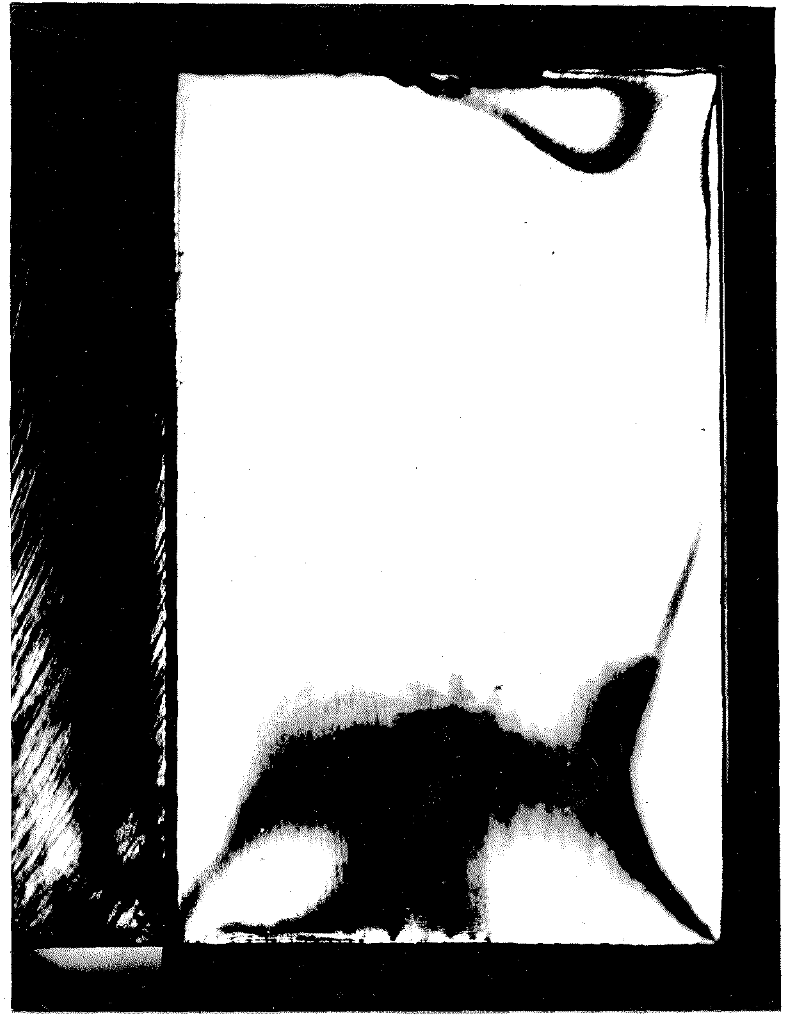

11 B $P = 2000$ lbs $\alpha = 77.5°$

12 B $P = 2000$ lbs $\alpha = 80°$

APPENDIX B.

Curves. From the results obtaind, the following curves are plotted:

Figs. 1 and 12	Evaluation of isochromatic lines for Type I and Type II loading respectively.
Figs. 2 and 13	Trajectories of the principal stresses for Type I and Type II loading respectively.
Figs. 3 and 14	n - x/h, curves for Type I and Type II loading respectively.
Figs. 4 and 5	Determination of the isotropic point for the Type I loading.
Figs. 6 and 16	Three dimentional diagrams of the principal stress -Q for Type I and II loading respectively.
Figs. 7 and 15	Three dimentional diagrams of the principal stress -P for Type I and II loading respectively.
Figs. 8 and 17	Three dimentional diagrams of the shearing stress τ_{xy} for Type I and II loading respectively.
Figs. 9,10,11	Contour lines of the principal stresses P,Q and the shearing stress τ_{xy} respectively, for Type I loading.

2,000 LBS.

EVALUATION OF
ISOCHROMATIC LINES

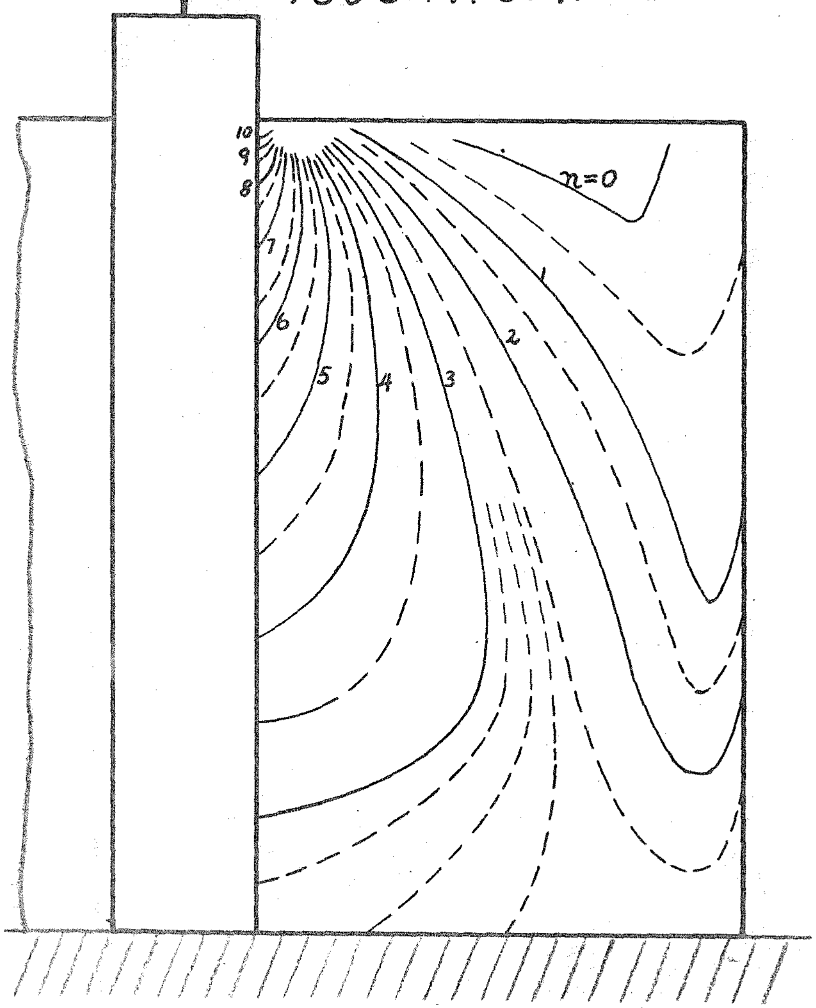

FIG. 1

2,000 LBS.

TRAJECTORIES OF THE
PRINCIPAL STRESSES

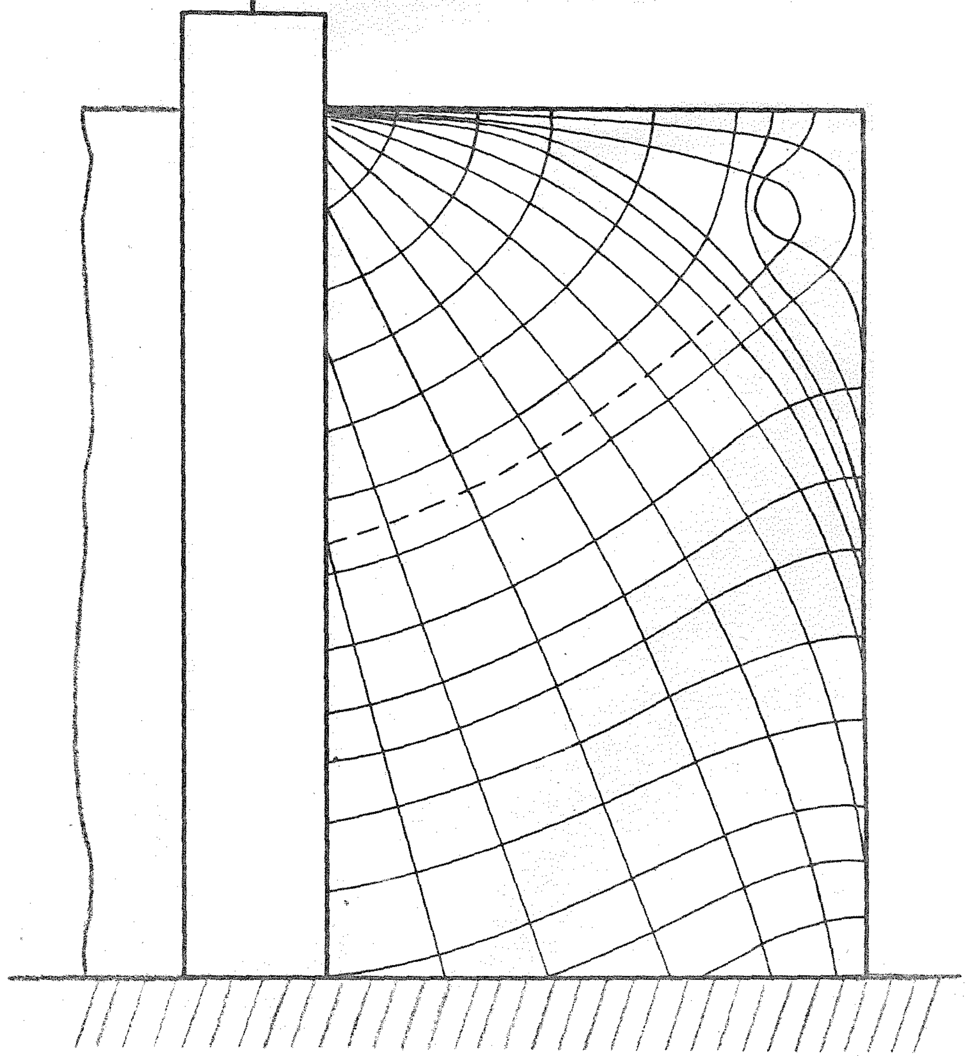

FIG. 2

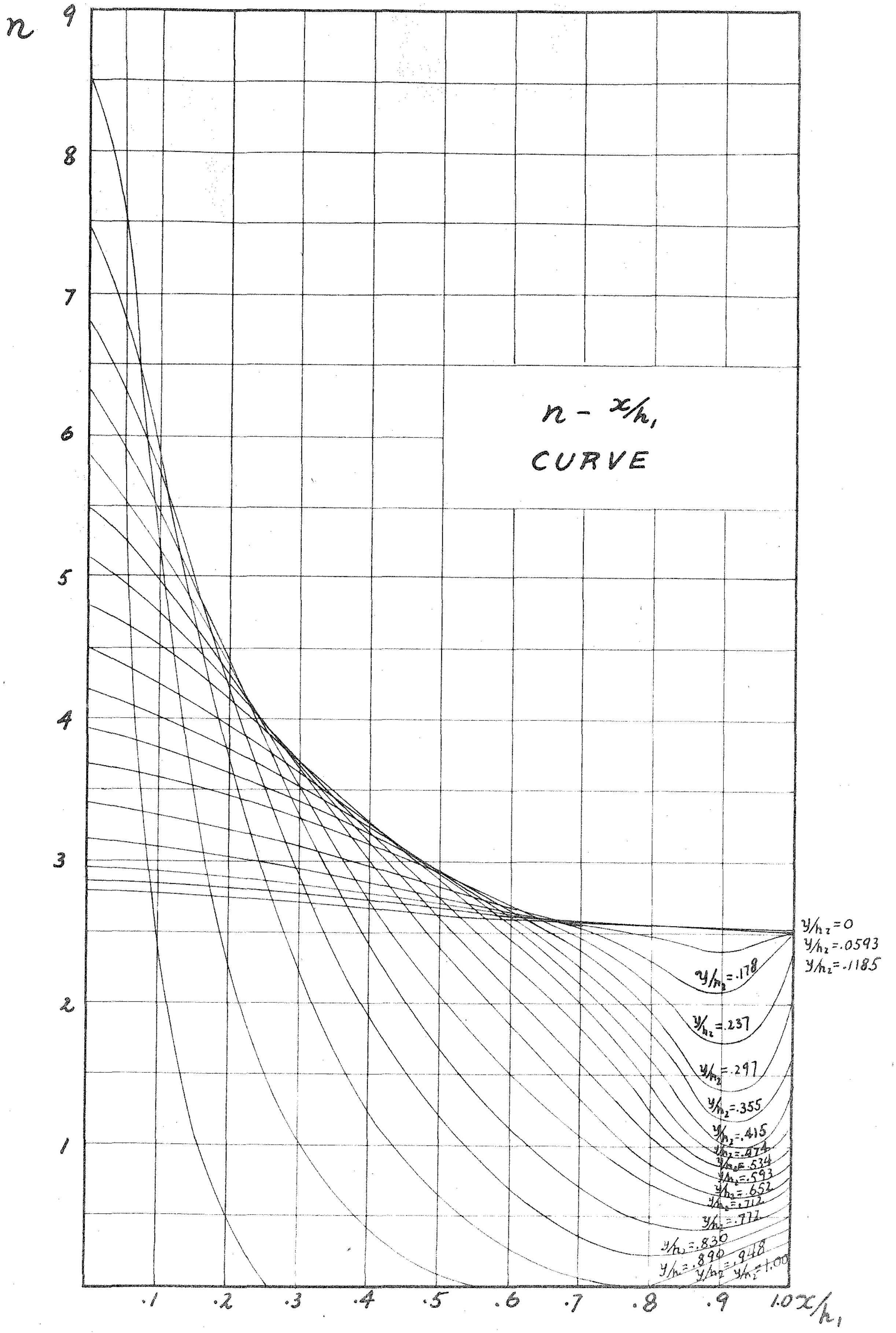
n
9
8
7
6
5
4
3
2
1
n - x/h1
CURVE
y/h2=0
y/h2=.0593
y/h2=.1185
y/h2=.178
y/h2=.237
y/h2=.297
y/h2=.355
y/h2=.415
y/h2=.474
y/h2=.534
y/h2=.593
y/h2=.652
y/h2=.712
y/h2=.771
y/h2=.830
y/h2=.890
y/h2=.948
y/h2=1.00
.1
.2
.3
.4
.5
.6
.7
.8
.9
1.0 x/h1

FIG. 3

DETERMINATION OF THE ISOTROPIC POINT

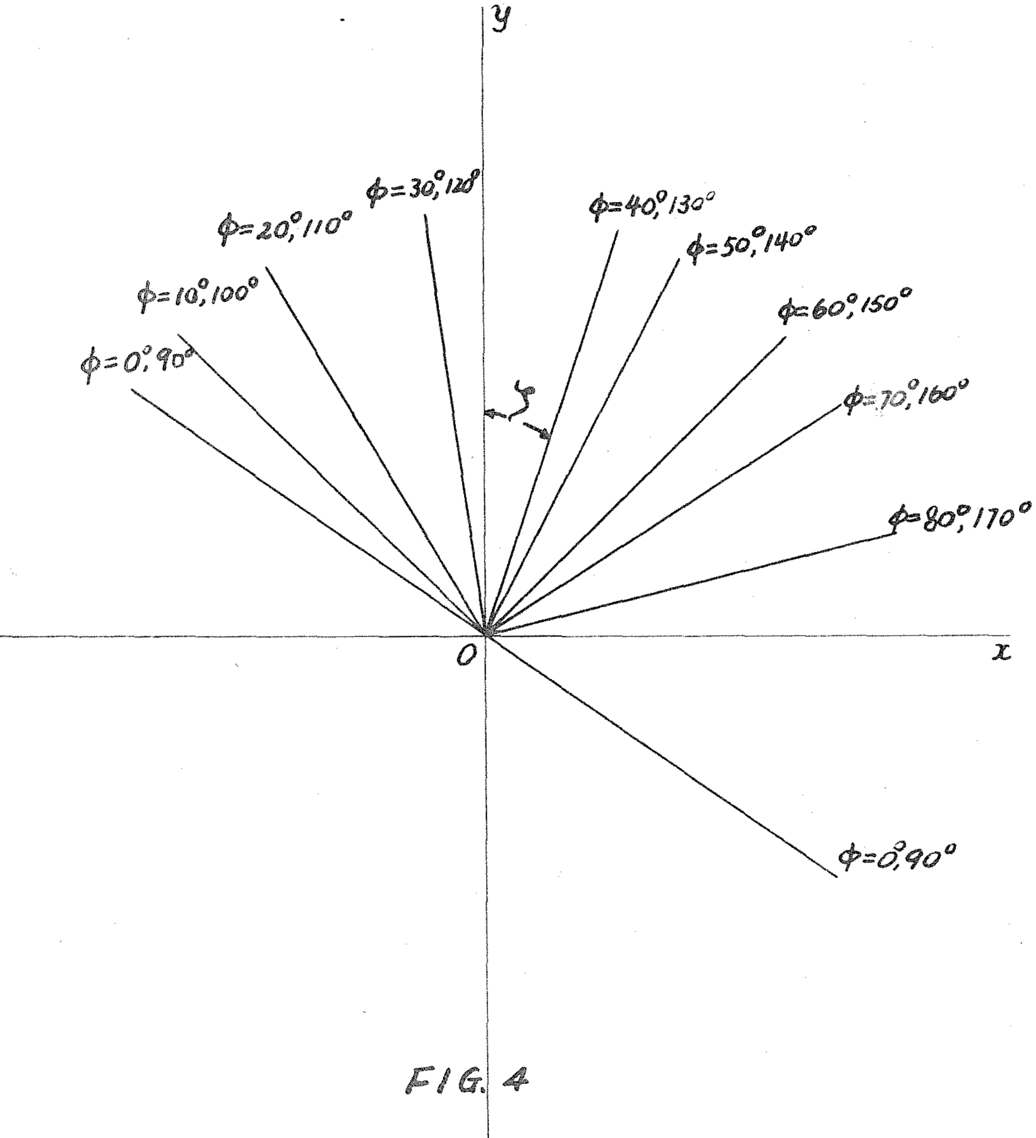

FIG. 4

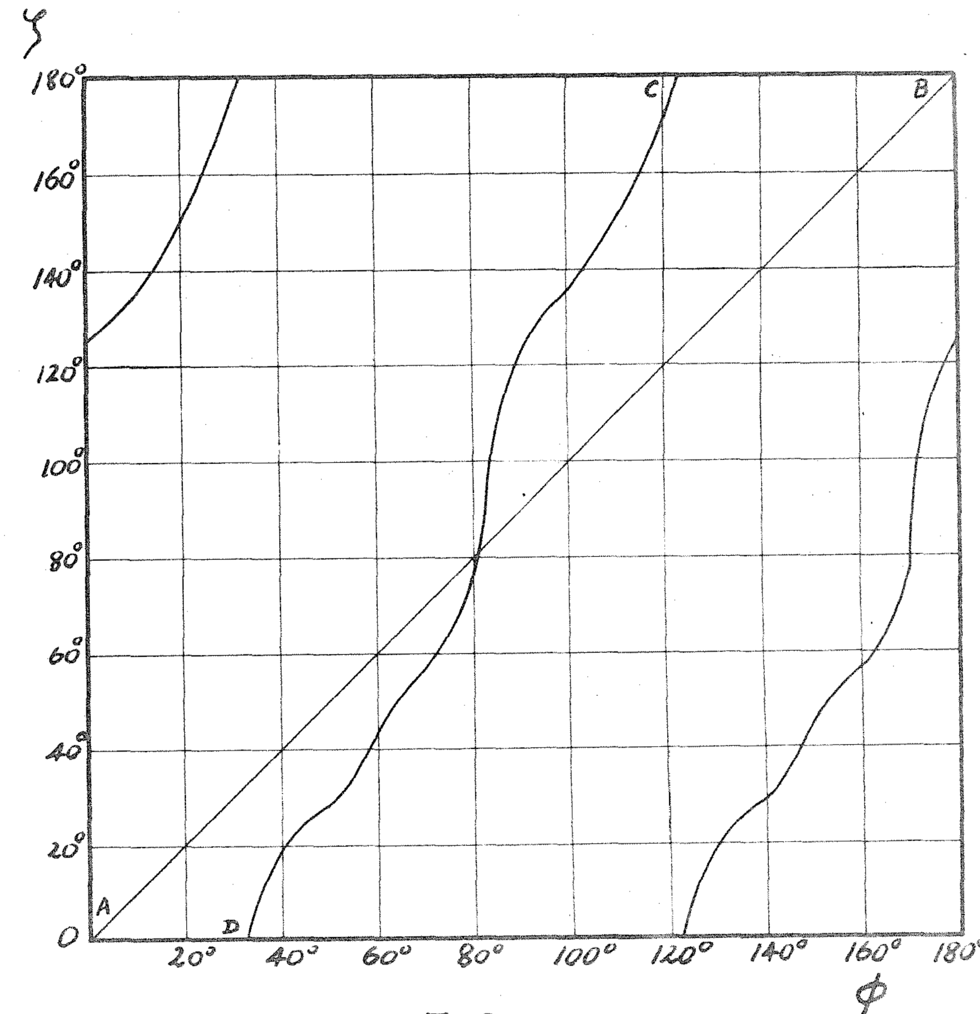

FIG. 5

THREE DIMENTIONAL DIAGRAM
OF THE PRINCIPAL STRESS Q

FIG. 6

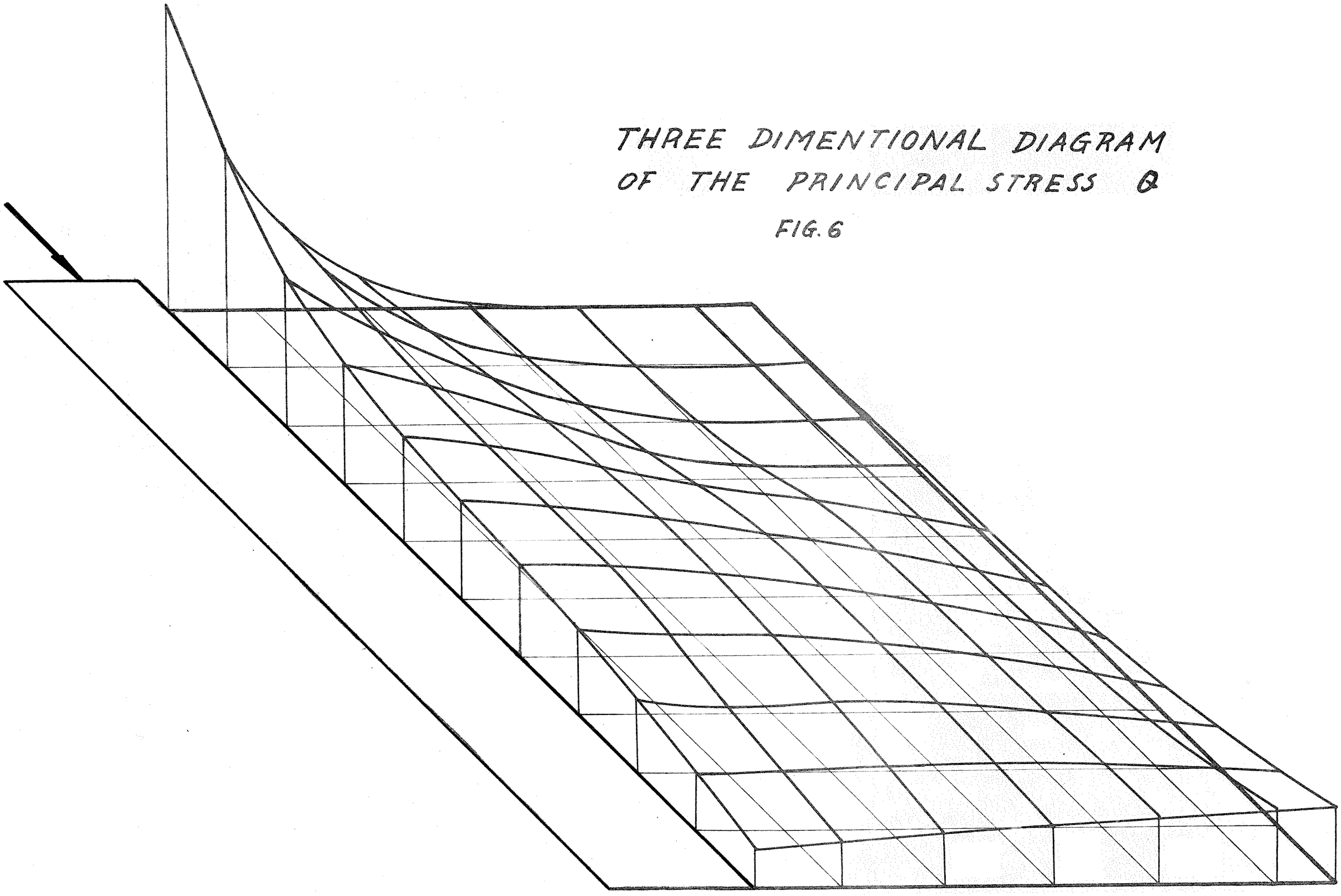

THREE DIMENTIONAL DIAGRAM
OF THE PRINCIPAL STRESS P

FIG. 7

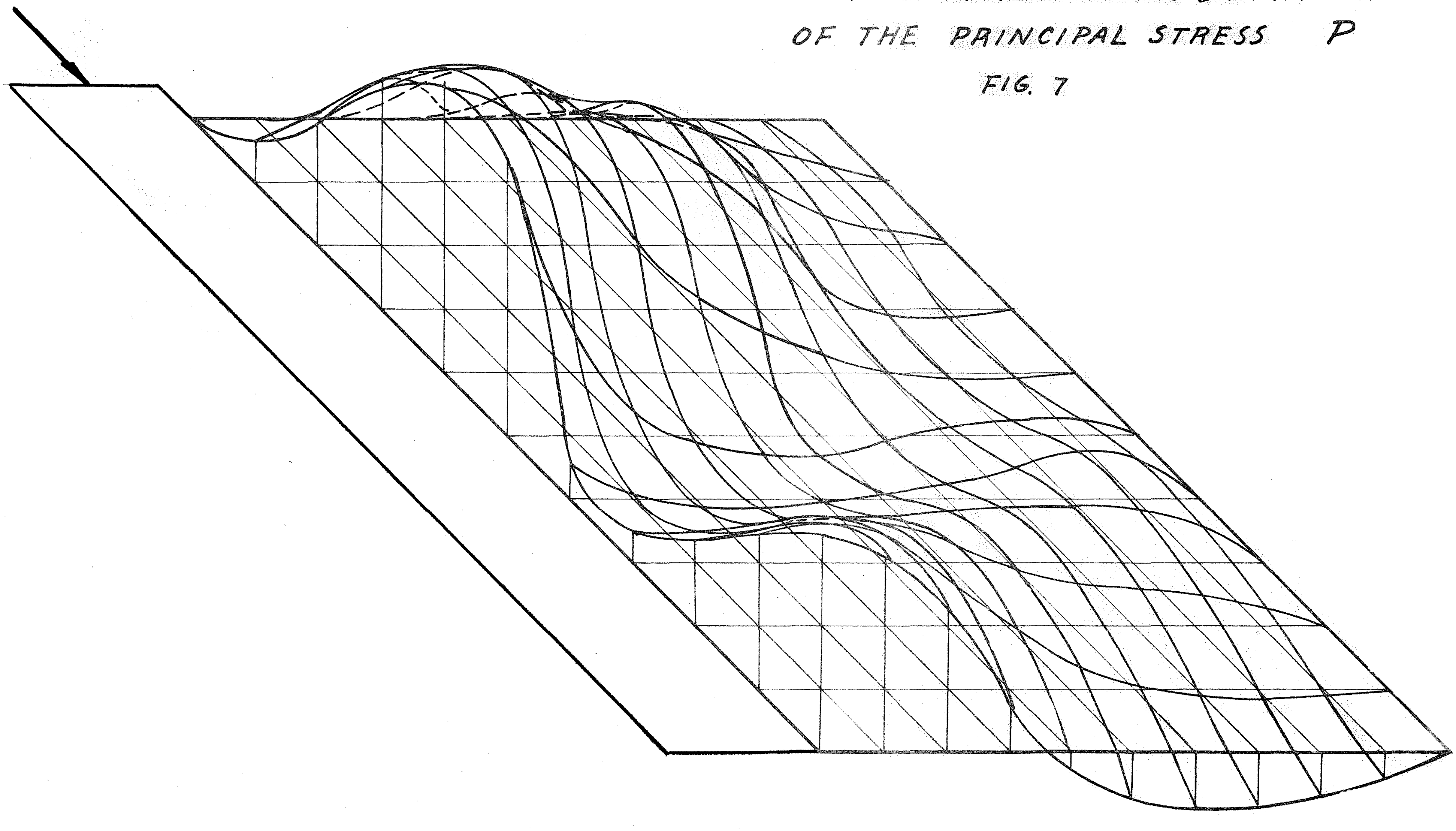

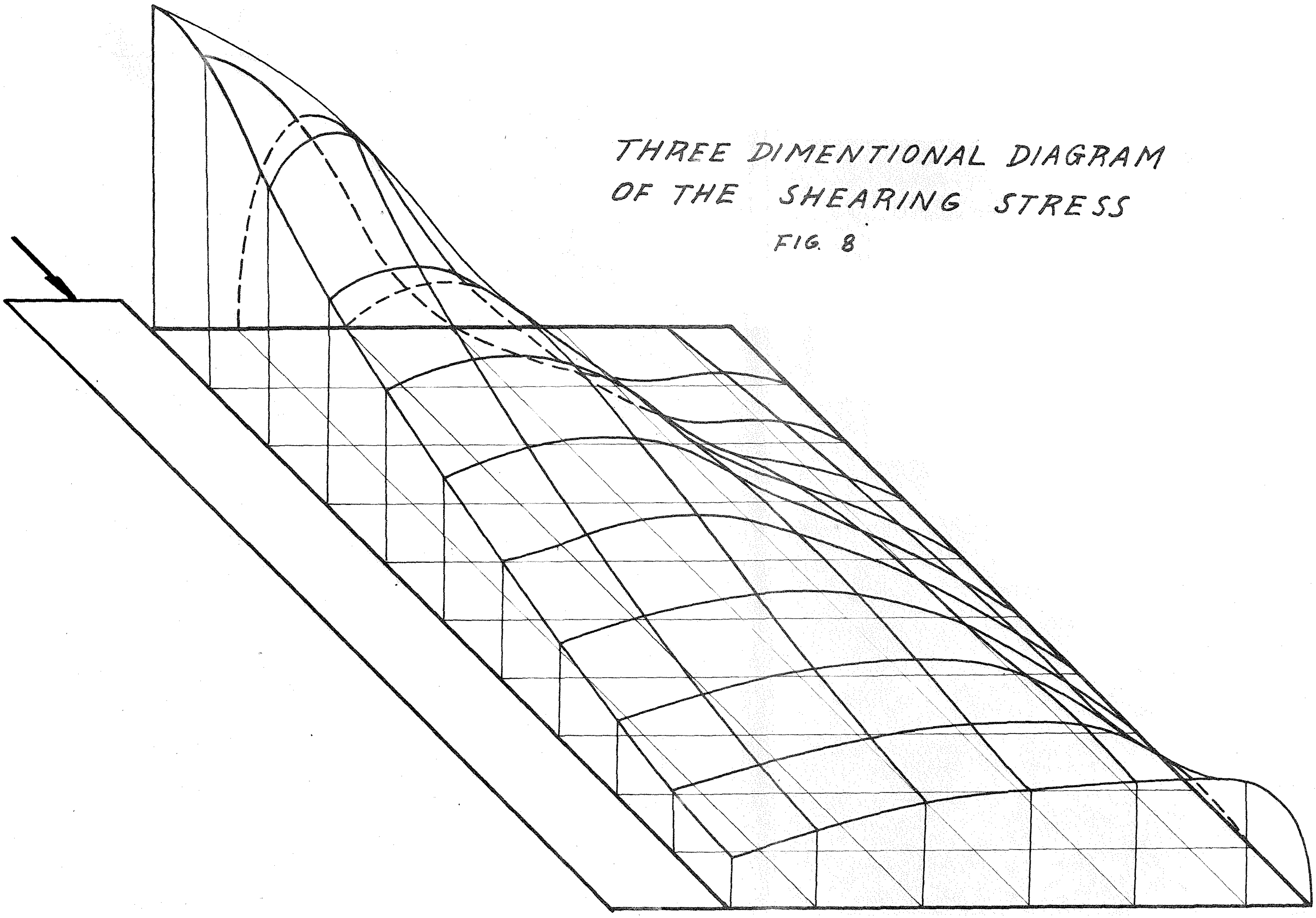

THREE DIMENTIONAL DIAGRAM
OF THE SHEARING STRESS
FIG. 8

CONTOUR LINES OF THE PRINCIPAL STRESS P

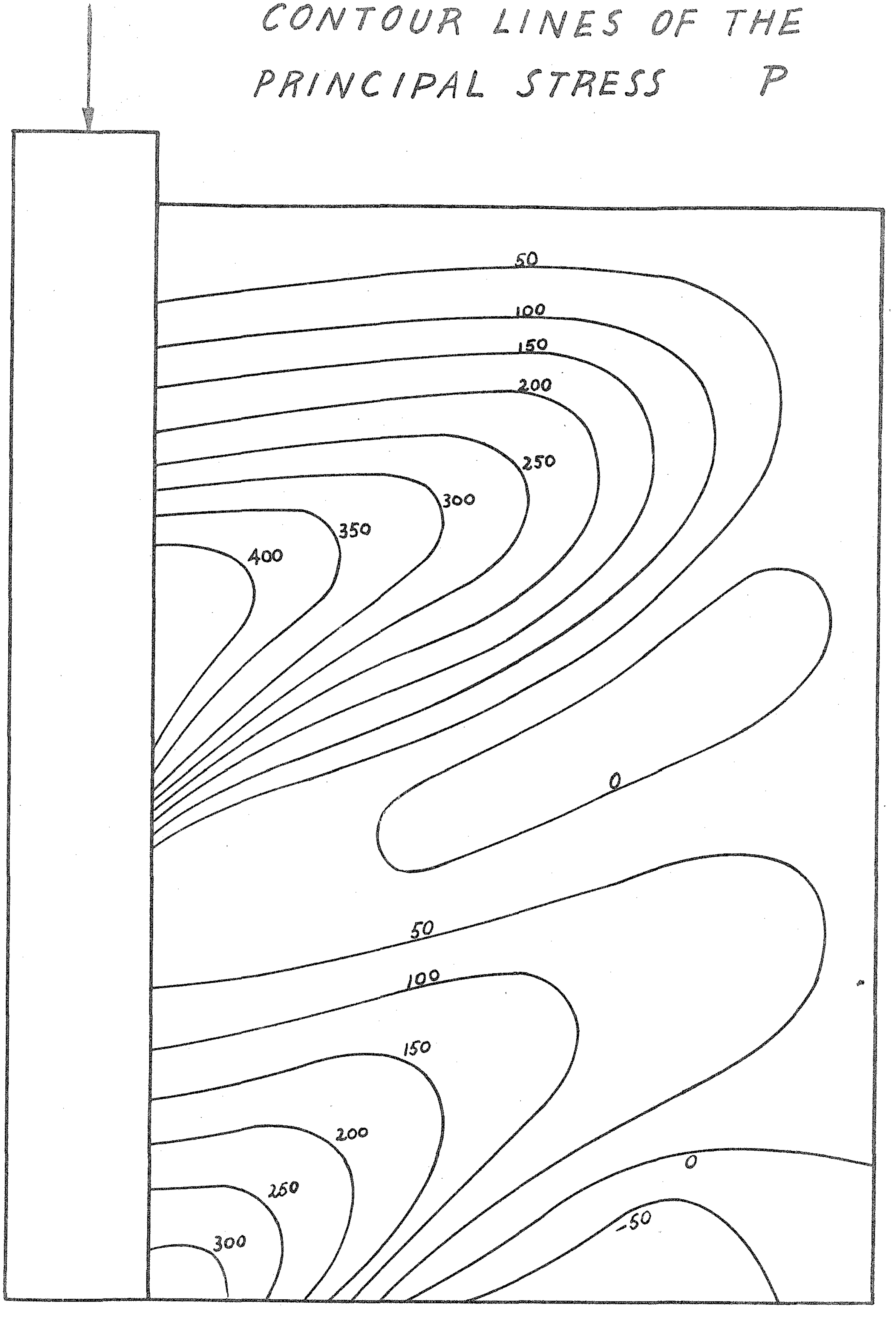

FIG. 9

CONTOUR LINES OF THE PRINCIPAL STRESS — Q

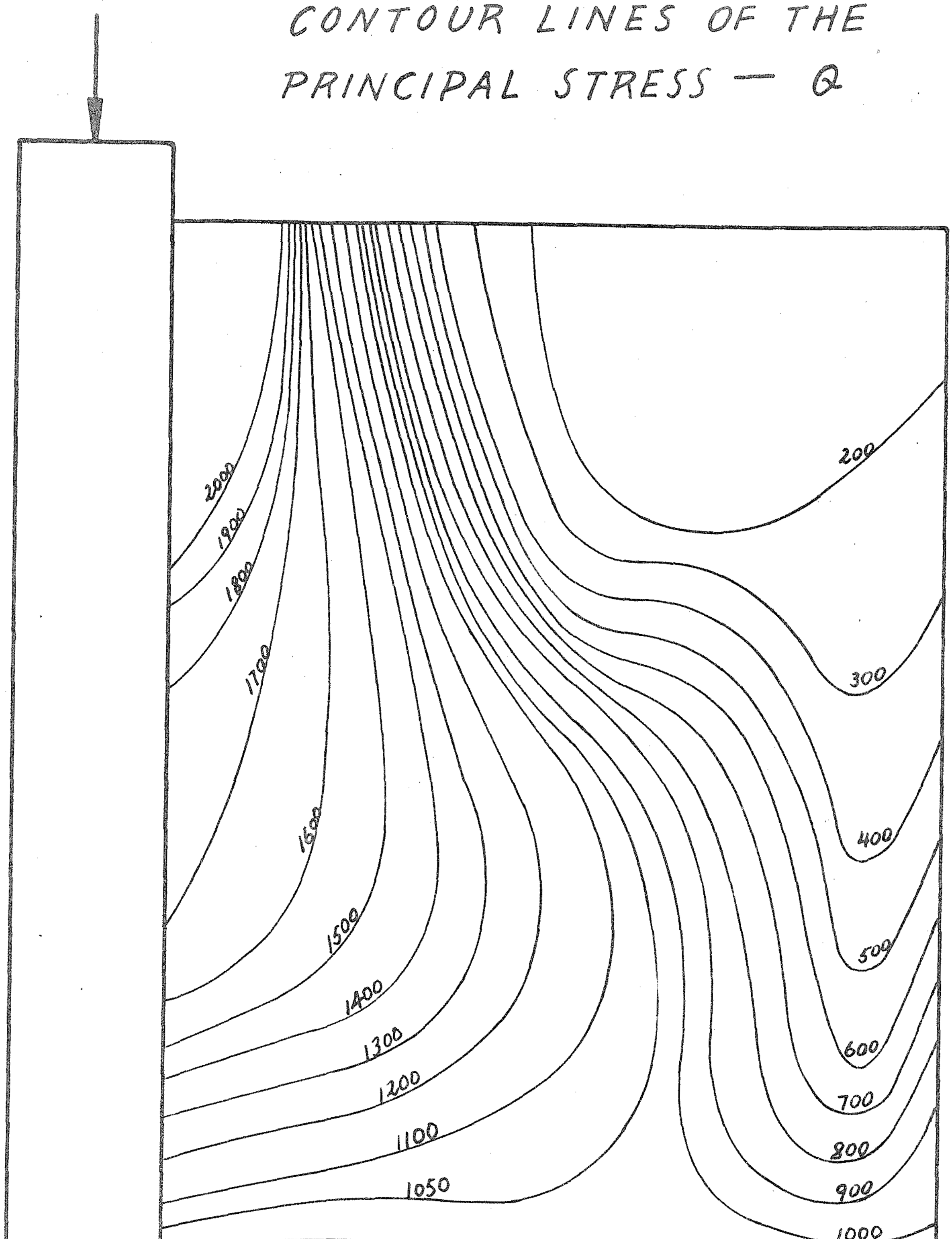

FIG. 10

CONTOUR LINES OF THE SHEARING STRESS

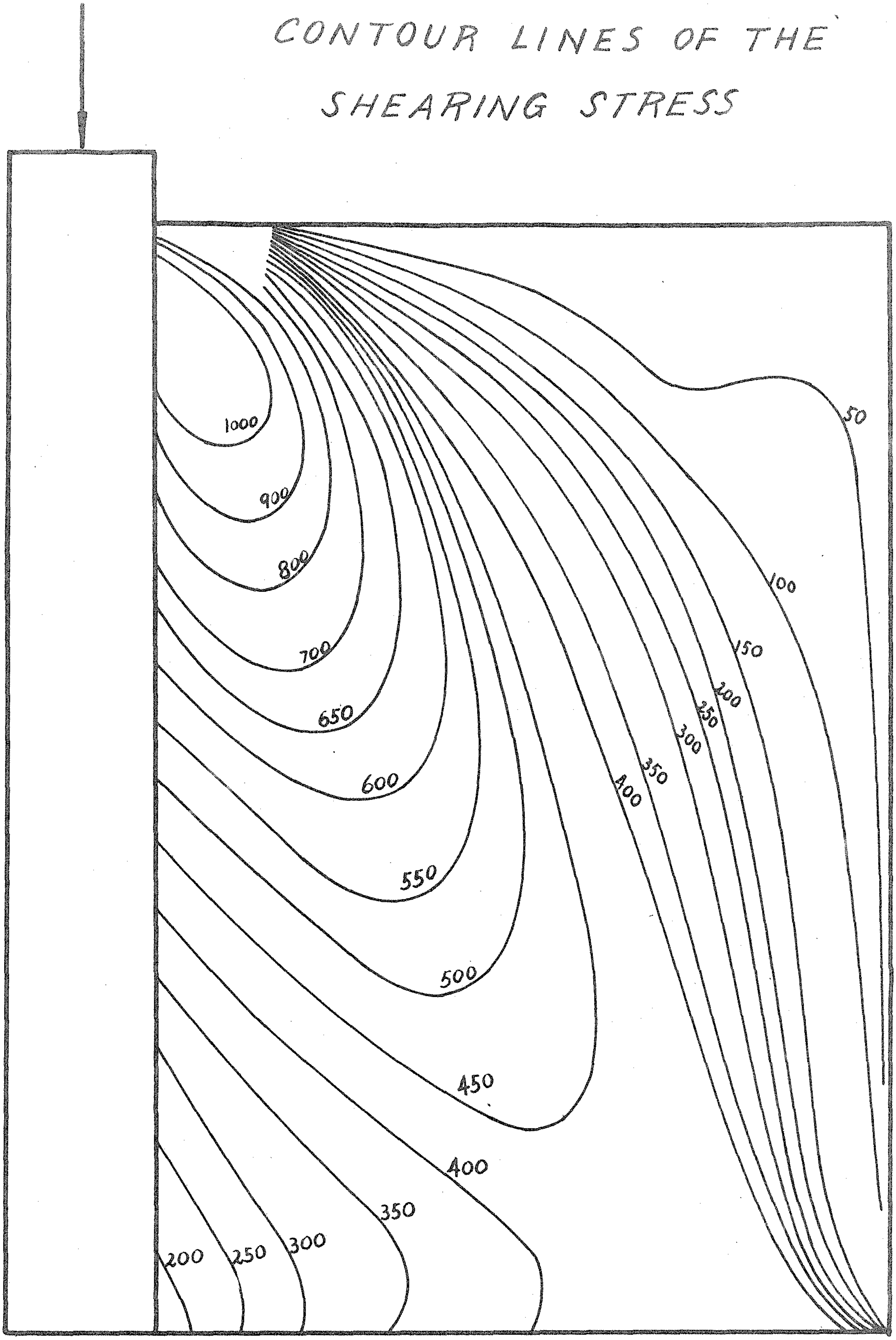

FIG. 11

EVALUATION OF ISOCHROMATIC LINES

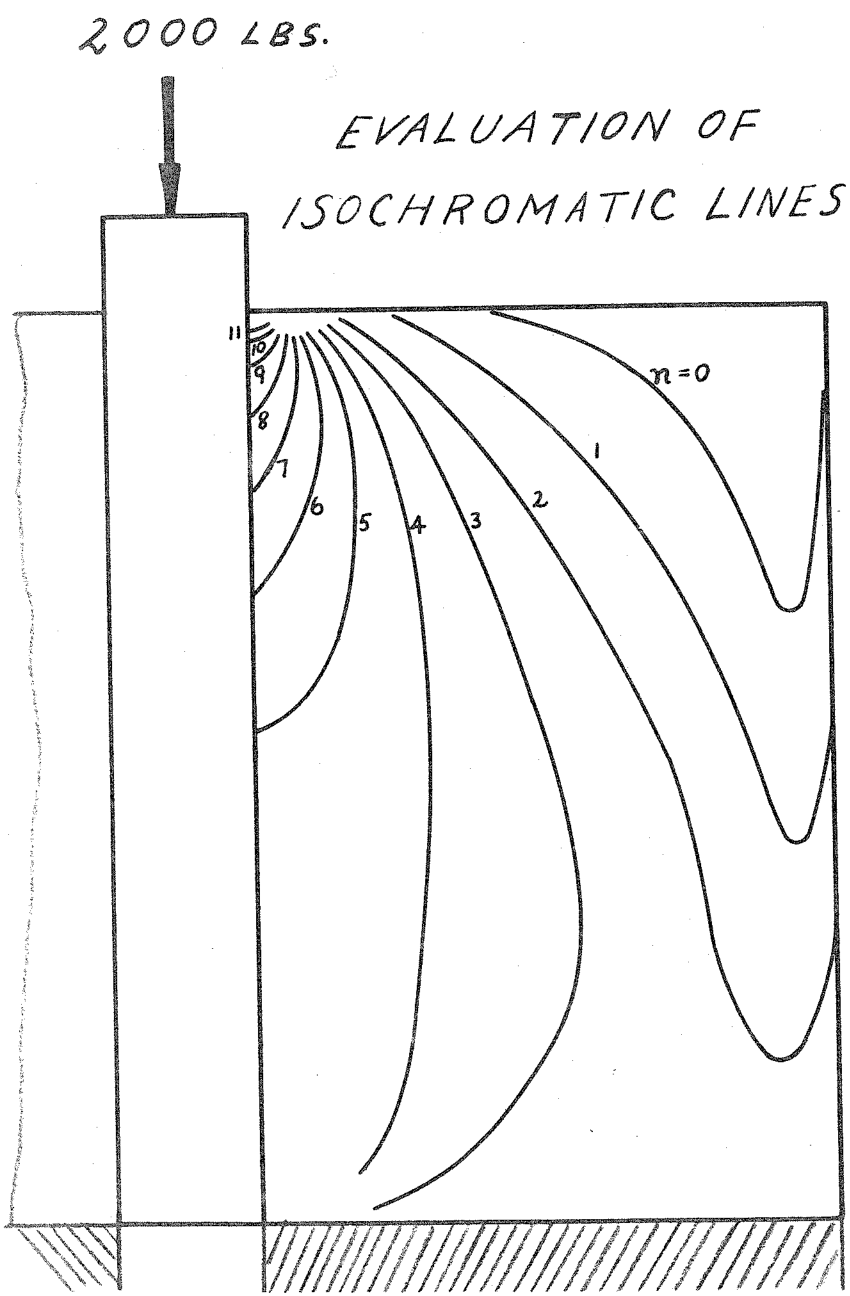

FIG. 12

TRAJECTORIES OF THE PRINCIPAL STRESSES

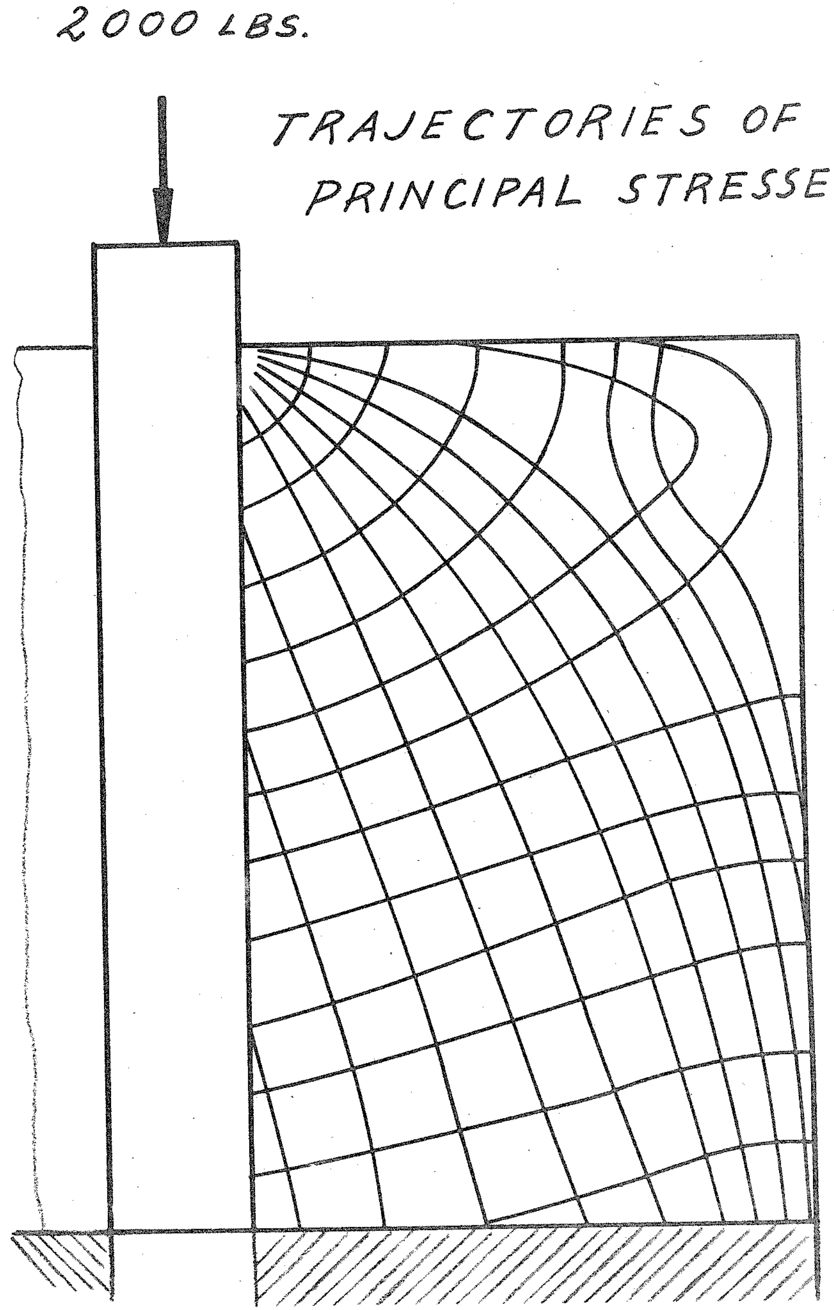

FIG. 13

$n - x/h_1$ CURVE

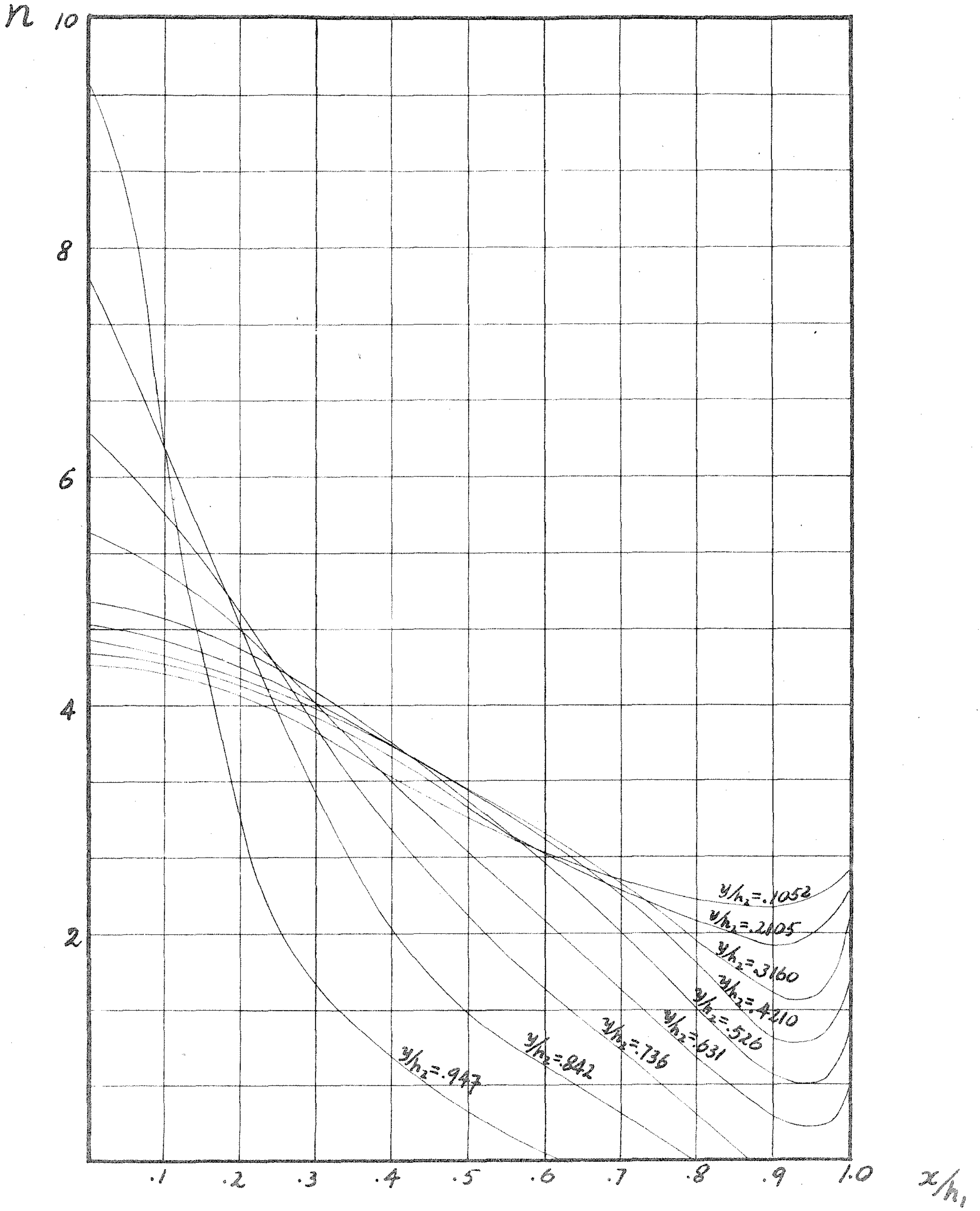

FIG. 14

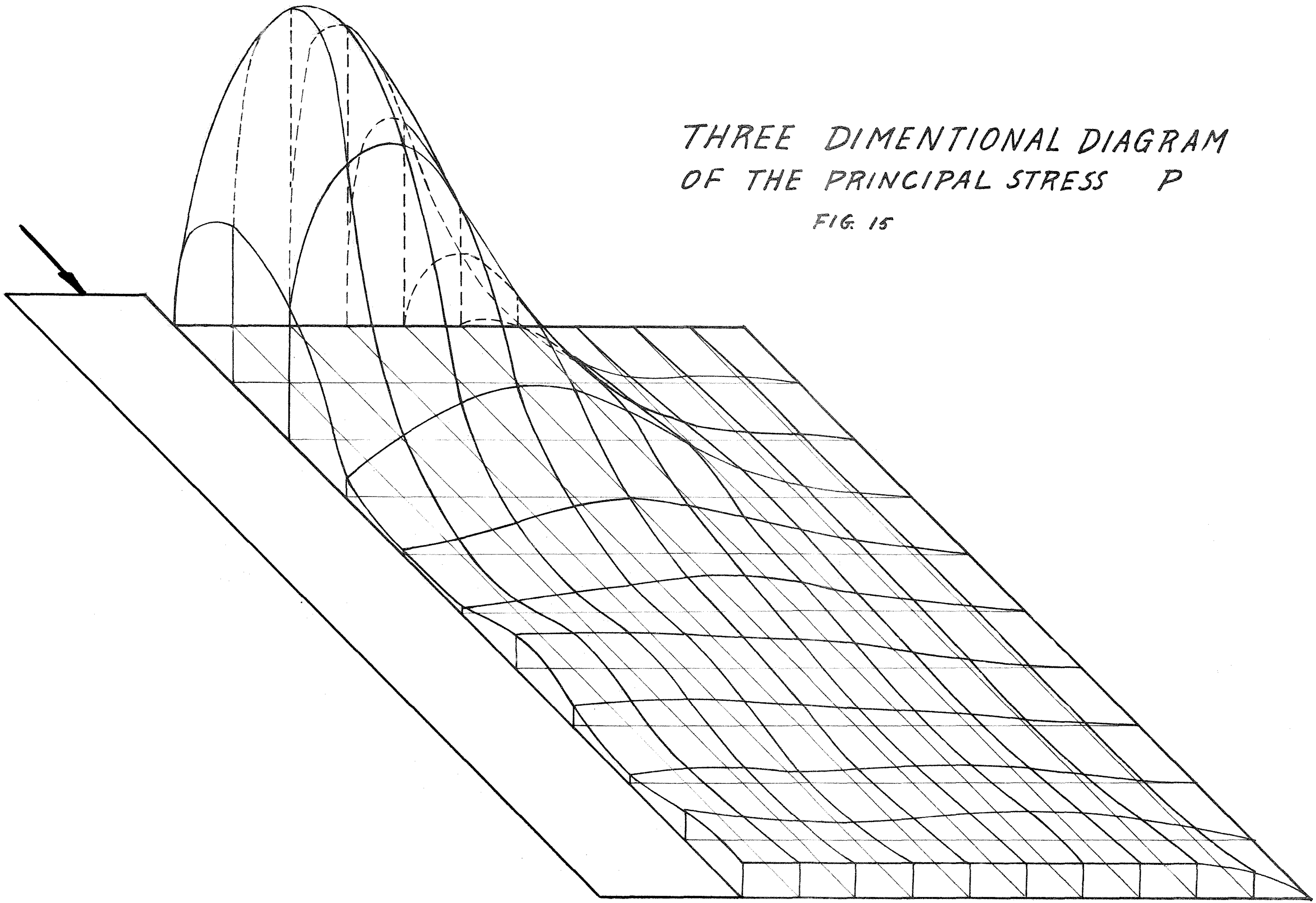

THREE DIMENTIONAL DIAGRAM OF THE PRINCIPAL STRESS P

FIG. 15

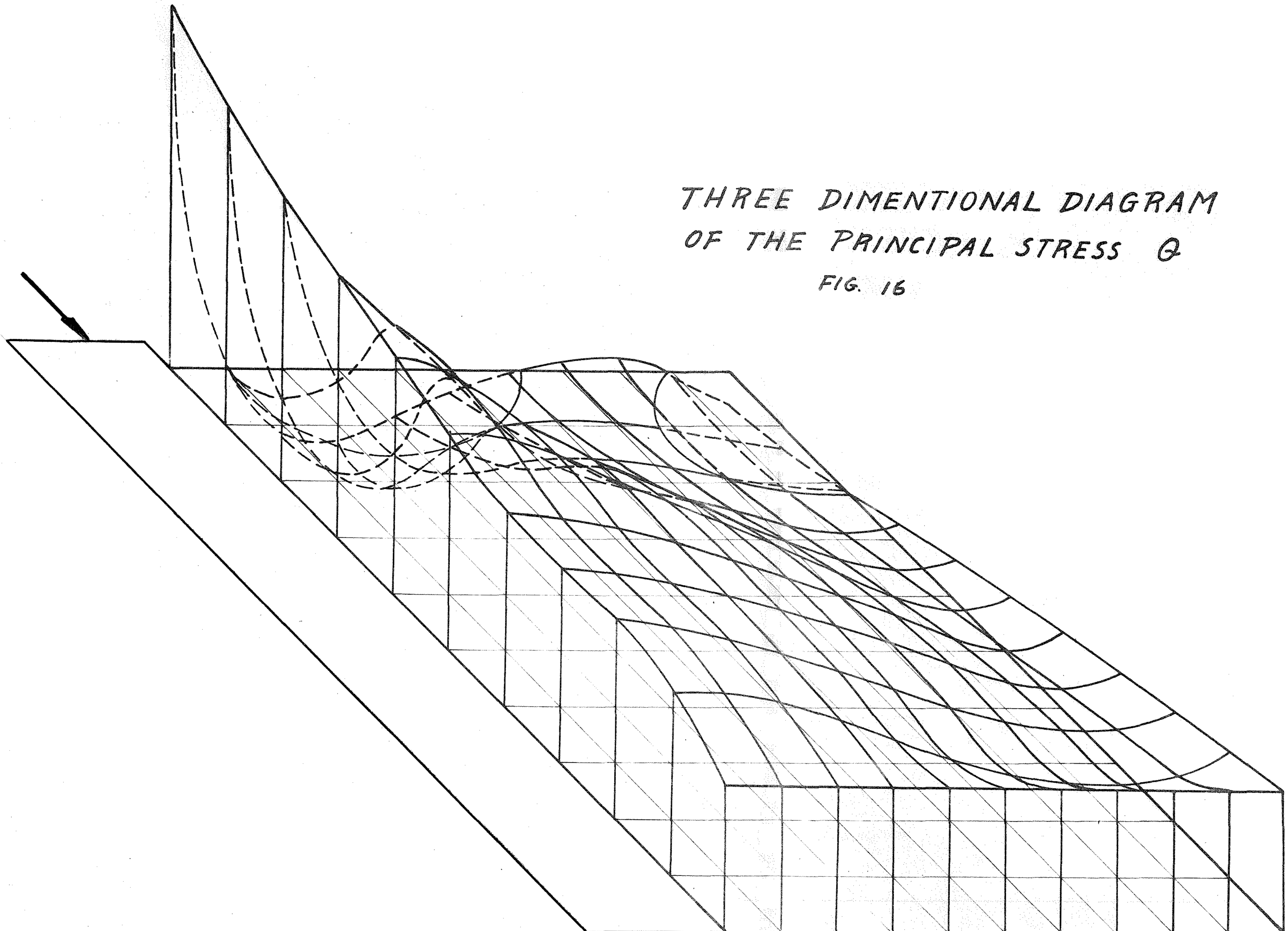

THREE DIMENTIONAL DIAGRAM OF THE PRINCIPAL STRESS Q

FIG. 16

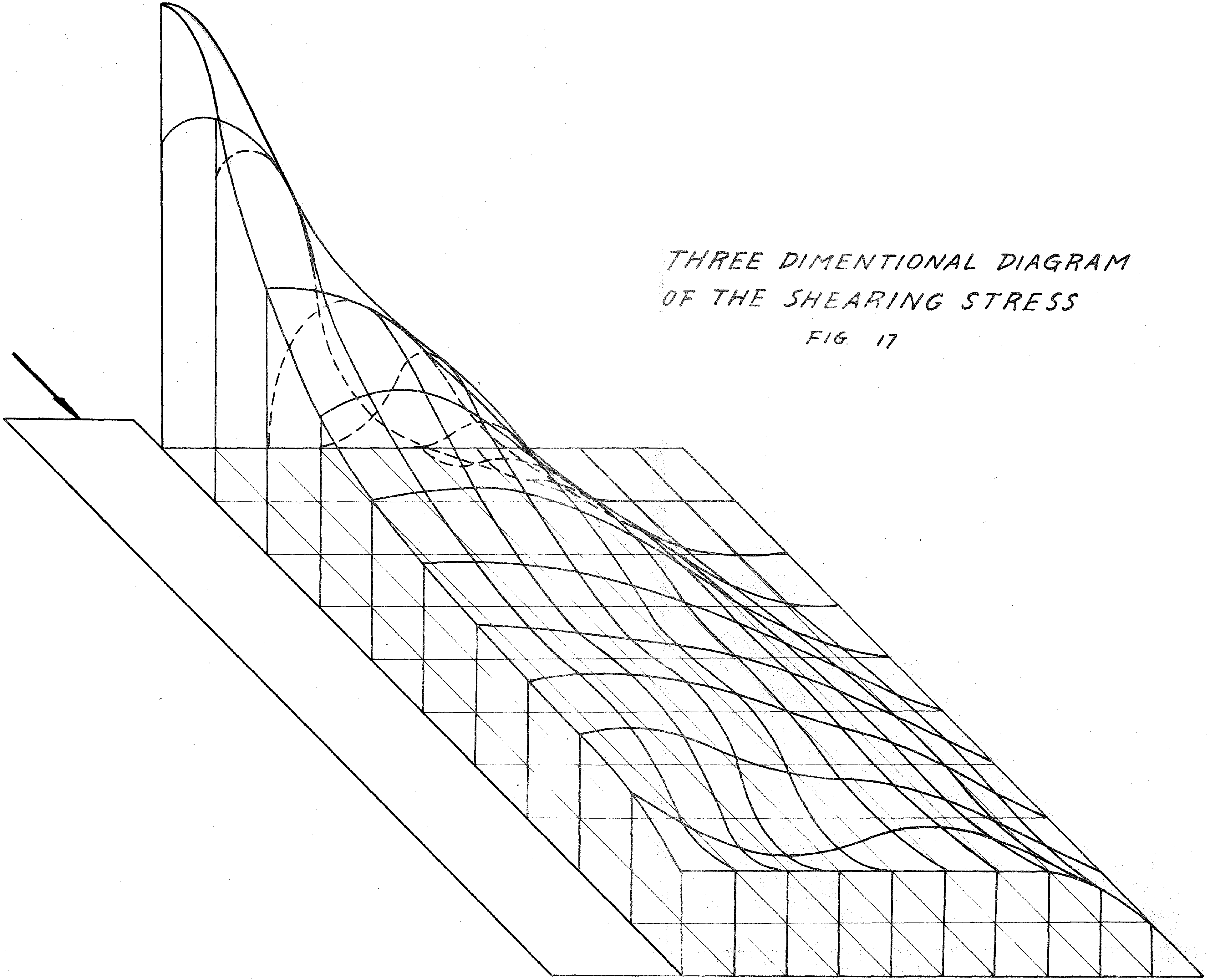

THREE DIMENTIONAL DIAGRAM
OF THE SHEARING STRESS
FIG. 17

APPENDIX C.

<u>Tables.</u> Results obtaind from the tests and calculations are tabulated.

Table 1	The integration of $(P-Q)\cot\psi$ along the lines of principal stress P for Type I loading.
Table II	The values of the principal stress Pand Q and the shearing stress calculated from table 1 for Type I loading.
Table III	The values of principal stress P,Q and shearing stress τ_{xy} obtaind by using the second method of integration, for Type II loading.

Table I.

INTEGRATION ALONG P-STRESS LINES

Line Number	(1) ϕ	(2) x/h_1	(3) y/h_2	(4) n	(5) ψ	(6) $\cot\psi$	(7) $(p-\theta)$	(8) $(p-\theta)\cot\psi$
1	80	.963	.070	2.50	98	-.1405	1033	-146
	75	.900	.061	2.52	108	-.3249	1041	-338
	70	.870	.055	2.53	124.5	-.6873	1046	-718
	60	.760	.0278	2.56	128	-.7813	1059	-826
2	80	.915	.133	2.30	92	-.0349	950	- 33.1
	75	.843	.122	2.39	92.5	-.0437	987	- 43.2
	70	.780	.111	2.50	100	-.1763	1034	-182.4
	60	.633	.067	2.61	106	-.4877	1078	-526
3	80	.907	.198	1.97	80	.1763	815	144
	75	.824	.185	2.17	81	.1584	896	223
	70	.740	.172	2.41	60.2	.5820	996	440
	60	.537	.117	2.66	102	-.2126	1100	-234
4	80	.925	.296	1.40	64.5	.4770	579	277
	75	.855	.286	1.90	55	.7002	786	551
	70	.720	.257	2.39	49	.8693	975	846
	60	.463	.191	2.82	77	.2309	1165	267
	70	.315	.158	2.90	118	-.5317	1200	-638
	75	181.5	.133	2.97	107.5	-.3153	1230	-388
5	80	.966	.395	1.06	68	.4040	439	177.5
	75	.925	.389	1.07	52.5	.7673	443	341
	70	.740	.355	2.08	56	.6745	860	580
	60	.435	.267	3.00	61.5	.5430	1240	674
	70	.300	.236	3.11	101	-.3000	1288	-386
	75	.129	.206	3.16	96	-.1051	1309	-137.5
6	80	.990	.527	.97	75.5	.2586	401	103.9
	60	.444	.347	3.06	51	.8098	1266	1024
	70	.268	.300	3.37	98.5	-.1495	1395	-209
	75	.102	.269	3.50	92	-.0349	1450	- 50.6
7	80	1.000	.628	.81	90	.0000	334	0
	70	.852	.580	.89	52	.7813	368	287
	60	.485	.425	2.95	41	1.1504	1220	1405
	70	.241	.356	3.55	88.5	.0262	1470	38.5
	75	.065	.318	3.75	96.5	-.1139	1552	-176.7
8	60	.577	.545	2.41	29	1.8040	994	1794
	70	.196	.420	3.82	92	-.0349	1580	- 55.2
	75	.020	.388	4.07	99	-.0699	1685	-117.9
9	60	.361	.567	3.36	106	-.2867	1388	-398
	70	.139	.498	4.26	92	-.0349	1760	- 61.5
	75	.000	.466	4.50	91	-.0175	1860	- 33.0

Table I (continued)

Line Number	(1) ϕ	(2) x/h_1	(3) y/h_2	(4) n	(5) ψ	(6) $\cot\psi$	(7) $(p-\theta)$	(8) $(p-\theta)\cot\psi$
10	50	.520	.733	1.82	150	-1.7321	753	-1306
	60	.268	.628	3.27	111	-.3839	1352	- 519
	70	.065	.574	4.85	95.5	-.0965	2010	- 193.6
11	40	.485	.840	1.20	140	-1.1918	496	- 592
	50	.333	.746	3.13	120	-.5774	1295	- 748
	60	.185	.688	4.50	98	-.1405	1860	- 261
	70	.0248	.640	5.35	95.5	-.0963	2210	- 213
12	30	.361	.900	1.55	127.5	-.7673	641	- 492
	40	.297	.837	2.85	117	-.5206	1179	- 614
	50	.213	.790	4.24	104	-.2493	1751	- 437
	60	.1165	.750	5.26	93	-.0524	2175	- 114
	70	-	.710	6.00	92	-.0349	2480	- 86.5
13	20	.245	.946	1.55	106.5	-.2962	641	- 190
	30	.213	.911	2.93	103	-.2309	1212	- 280
	40	.176	.880	4.36	97.5	-.1317	1802	- 237
	50	.116	.840	5.50	95.5	-.0963	2270	- 219
	60	.0463	.811	6.26	92.5	-.0437	2590	- 113.2
14	10	.0925	.980	3.75	93	-.0524	1550	- 81.5
	20	.0833	.970	4.65	92.5	-.0437	1922	- 84
	30	.0740	.947	6.43	90	.0000	2600	- 0
	40	.0555	.932	6.90	92	-.0349	2850	- 99.5
	50	.0150	.910	7.65	94	-.0699	3160	- 221
	60	-	.887	7.70	95	-.0875	3180	- 278

Table II.

Line Number	(1) ϕ	(2) x/h_1	(3) y/h_2	(4) n	(5) $(P-\theta)$	(6) P	(7) θ	(8) $\sin 2\alpha$	(9) τ_{xy}
1	18°	.889	.06	2.53	1045	-42.4	-1087.4	.5878	-307.5
	24°	.704	.006	2.56	1057	-92.0	-1149	.7431	-392.5
2	12°	.889	.131	2.5	1032	-2.36	-1034.4	.4067	-209.5
	27°	.704	.089	2.55	1052	-30.2	-1082.2	.8090	-426.0
	23°	.519	.033	2.55	1052	-29.2	-1081.2	.7193	-378.5
3	12°	.889	.194	2	826	23.6	- 802.4	.4067	-168.0
	21.5°	.704	.161	2.53	1045	37.7	-1007.3	.6820	-356.5
	25°	.519	.106	2.67	1102	35.3	-1066.7	.7660	-422.0
	22°	.333	.061	2.77	1144	134.5	-1009.5	.6947	-397.0
	14°	.148	.027	2.81	1160	274.5	- 885.7	.4695	-272.0
4	14°	.889	.283	1.55	640	57.1	- 582.9	.4695	-150.0
	22°	.704	.255	2.43	999	83.5	- 915.5	.6947	-346.5
	26°	.519	.210	2.76	1139	83.5	-1055.5	.7880	-448.0
	19°	.333	.161	2.97	1228	190.0	-1038	.6157	-378.0
	15°	.148	.125	2.98	1232	228.0	-1004	.5000	-308.0
	10°	-.037	.100	2.95	1220	247.5	- 972.5	.3420	-208.5
5	17°	.889	.384	1.33	549	47.2	- 501.8	.5592	153.5
	25°	.704	.347	2.25	930	55.6	- 878.4	.7660	356.0
	27°	.519	.293	2.84	1174	55.2	-1118.8	.8090	475.0
	20°	.333	.244	3.12	1290	121.2	-1168.8	.6125	414.0
	16°	.148	.211	3.17	1312	144.3	-1167.7	.5299	347.0
	11°	-.037	.180	3.18	1314	152.4	-1161.6	.3746	246.4
6	20°	.889	.487	.92	380	28.3	- 361.7	.6425	122.1
	27°	.704	.436	2.06	852	27.8	- 824.2	.8090	344.3
	26°	.519	.373	2.85	1178	39.6	-1148.4	.7880	464.0
	24°	.333	.313	3.28	1356	50.1	-1305.9	.7431	504.0
	17°	.148	.277	3.47	1434	76.9	-1357.1	.5592	461.0
	12°	-.037	.253	3.52	1454	79.3	-1374.7	.4067	295.5
7	23°	.889	.566	.81	335	-.943	- 335.9	.7193	120.3
	28°	.704	.505	1.9	785	-3.300	- 788.3	.8290	325.3
	27°	.519	.433	2.82	1165	.472	-1164.5	.8090	471.0
	25°	.333	.377	3.4	1406	5.650	-1400.3	.7660	538.0
	18°	.148	.333	3.65	1510	18.400	-1491.6	.5878	444.0
	13°	-.037	.306	3.8	1570	26.900	-1543.1	.4380	344.0
8	26°	.889	.666	.64	264	- .472	- 264.5	.7880	104.1
	29°	.704	.598	1.53	632	-2.83	- 634.8	.8480	268.0
	28°	.519	.522	2.68	1108	- .943	-1108.9	.8290	458.5
	27°	.333	.457	3.50	1447	.943	-1446	.8090	584.5
	19°	.148	.422	3.97	1640	12.25	-1627.7	.6157	506.0
	14°	-.037	.378	4.10	1695	17.45	-1687.5	.4695	398.0

Table II (continued)

Line Number	(1) ϕ	(2) x/h_1	(3) y/h_2	(4) n	(5) $(P-Q)$	(6) P	(7) Q	(8) $\sin 2\alpha$	(9) τ_{xy}
10	90°	.759	1.00			0	-1032	0	0
	65°	.703	.861	.18	74.3	92	-17.7	.7660	28.45
	50°	.519	.734	.18	743	347.5	-295.5	.9848	365.4
	33°	.333	.646	3.44	1421	715.0	-1290	.9135	648.5
	24°	.148	.587	4.48	1851	790.0	-1061.0	.7431	687.0
	16°	-.037	.547	4.93	2040	816.0	-1775	.5299	540.0
11	90°	.639	1.000	-.43		0		0	0
	51°	.519	.866	.78	322	1156.5	- 165.5	.9781	157.5
	40°	.333	.745	3.14	1298	293.5	-1004.5	.9848	638.0
	27°	.148	.672	4.80	1982	384.0	-1598	.8090	802.0
	17°	-.037	.627	5.43	2245	424.0	-1821	.5592	627.0
12	90°	.407	1.000	-.43		0		0	0
	55.5°	.333	.866	2.15	887	129.7	-757.3	.9336	414.0
	33°	.148	.759	4.95	2044	322.0	-1722.0	.9135	934.0
	18°	-.037	.707	5.85	2416	348.5	-2067.5	.5878	710.0
13	90°	.259	1.000	0		0		0	0
	44°	.148	.855	4.95	2044	145.2	-1898.8	.9994	102.1
	19°	-.037	.792	6.75	2790	203	-2587	.6157	859.0

Table III.

(1) x/h_1	(2) y/h_2	(3) τ_{xy}	(4) $(\sigma_x-\sigma_y)$	(5) σ_x	(6) σ_y	(7) $(P+Q)$	(8) $(P-Q)$	(9) P	(10) Q
1.0	.1	0	1100	0	-1100	-1100	1118	9.[illegible]	-1109
.9	"	126.7	914	21.5	-8925	- 871.0	960	44.5	-9155
.8	"	233.3	830	49.4	-7806	-731.0	943	106.0	-837. 0
.7	"	310.0	810	66.7	-743.3	-676.6	1000	161.7	-838.3
.6	"	354.6	865	74.85	- 790.2	-715.35	1095	189.8	-905.2
.5	"	352.0	1015	84.00	- 931	-947	1210	131.5	-1078.5
.4	"	273.3	1230	87.6	-1142.4	-1054.8	1350	147.6	-1202.4
.3	"	253.3	1473.0	81.4	-1391.6	-1310.2	1518	103.9	-1414.1
.2	"	285.3	1568.5	63.4	-1505.1	-1441.7	1671.1	114.7	-1556.4
.1	"	366.7	1559	41.3	-1517.7	-1476.4	1756	139.8	-1616.2
0	"	504.0	1490	27.0	-1463	-1436.0	1800	182.0	-1618.0
1.0	.2	0	958	0	- 958	- 958	958	0	- 958
.9	"	82.7	835	2.93	- 832.1	- 829.2	842	6.4	-835.6
.8	"	179.4	798	10.72	-787.3	- 776.6	871	47.2	- 823.8
.7	"	274.0	822	15.95	-806	- 790.0	970	90.0	- 880.0
.6	"	326.0	917	14.64	-902	- 887.4	1120	116.3	-1003.7
.5	"	346.6	1080	4.88	-1075	-1070.1	1282	105.95	-1176.0
.4	"	368.0	1243	- 6.51	-1249.5	-1256.0	1446	95.0	-1351.0
.3	"	420.7	1345	-24.44	-1369.4	-1393.8	1520	63.1	-1456.9
.2	"	512.0	1410	-51.1	-1461.1	-1512.2	1710	98.9	-1611.1
.1	"	534.7	1458	-84.4	-15424	-1627.8	1792	82.1	-1709.9
0	"	516.7	1528	-103.0	-1631.0	-1734	1841	53.5	-1787.5
1.0	.3	0	810	0	-810	- 810	810	0	- 810
.9	"	96.0	650	- 4.88	-654.9	- 659	700	20.5	- 679.5
.8	"	200.0	671	-11.07	-682.1	- 693.2	770	38.4	- 731.6
.7	"	281.3	802	-14.00	-816.0	- 830	965	67.5	- 897.5
.6	"	340.7	934	-19.52	-953.5	- 973	1180	103.5	-1076.5
.5	"	405.7	1047	-35.8	-1082.8	-1118.5	1330	105.7	-1224.3
.4	"	475.4	1146	-42.9	-1188.9	-1231.8	1480	124.1	-1355.9
.3	"	518.6	1253	-40.7	-1293.7	-1334.4	1634	149.8	-1484.2
.2	"	540.0	1362	-37.1	-1399.1	-1436.0	1749	156.5	-1592.5
.1	"	542.0	1465	-32.2	-1497.2	-1529.4	1828	149.3	-1678.7
0	"	524.7	1552	-29.3	-1581.3	-1610.6	1869	129.2	-1739.8
1.0	.4	0	658	0	- 658	-658	658	0	- 658
.9	"	92.0	504	3.91	-500.1	-496.2	545	24.4	-520.6
.8	"	185.6	598	14.32	-583.7	-569.4	677	53.8	-623.2
.7	"	272.6	790	24.1	-765.9	-741.8	935	96.6	-838.4
.6	"	360.0	926	31.6	-894.4	-862.8	1166	151.6	-1014.4
.5	"	412.0	1063	36.8	-1026.2	-989.4	1345	177.8	-1167.2
.4	"	439.4	1220	28.1	-1181.9	-1143.8	1515	185.6	-1329.4
.3	"	466.6	1360	51.8	-1308.2	-1256.4	1670	206.8	-1463.2
.2	"	497.0	1482	55.8	-1426.9	-1371.8	1792	210.1	-1581.9
.1		519.0	1563	51.2	-1511.8	-1460.6	1879	209.2	-1669.8
0		537.3	1591	45.3	-1545.7	-1500.4	1920	209.8	-1710.2